Paleoceanography and Paleoclimatology

RESEARCH ARTICLE
10.1029/2025PA005355

# Evolution of the East Antarctic Ice Sheet Since Glacial Inception From Seismic Stratigraphic Records in Vincennes Bay

**Timo Mühlberger-Krause[1,2,3], Karsten Gohl[1], Katharina Hochmuth[3,4], German Leitchenkov[5,6], Chiara A. Tobisch[7], Rachel Barrett[7,8], Johann P. Klages[1,9], and Sebastian Krastel[7]**

[1]Alfred Wegener Institute Helmholtz-Centre for Polar and Marine Research, Division of Geosciences, Bremerhaven, Germany, [2]Department Geosciences, University of Bremen, Bremen, Germany, [3]Australian Centre for Excellence in Antarctic Science, Hobart, TAS, Australia, [4]Institute for Marine and Antarctic Studies, University of Tasmania, Hobart, TAS, Australia, [5]Department of Geophysics, St. Petersburg State University, St. Petersburg, Russia, [6]Scientific Research Institute for Geology and Mineral Resources of the World Ocean, St. Petersburg, Russia, [7]Kiel University, Institute of Geosciences, Kiel, Germany, [8]north.io GmbH, Kiel, Germany, [9]Cluster of Excellence 'The Ocean Floor - Earth's Uncharted Interface', University of Bremen, Bremen, Germany

**Abstract** Seismic reflection data from Vincennes Bay, East Antarctica, provide the first insights into the Cenozoic evolution of the East Antarctic Ice Sheet (EAIS) in the Knox Coast. Long-distance seismic horizon correlation allows age estimates for the seismic stratigraphic framework constructed for the continental shelf. Preglacial depositional patterns reveal extensive fluvial plains on the continental shelf from the Late Cretaceous until the latest Eocene (~34 Ma). These transitioned to glaciofluvial outwash plains during the late Oligocene. The earliest clear indication of ice sheets present on the Vincennes Bay continental shelf are two generations of large buried tunnel valley systems that developed during the Oligocene-Miocene Transition (~24 Ma) and early Miocene during meltwater-rich glaciations originating in the Knox Coastal Plain. Glacially transported sediment wedges deposited at the end of the early mid-Miocene (>~14 Ma) mark the beginning of steep glacial progradation of the continental shelf continuing through the Miocene and Pliocene. Ice sheet development from the late mid-Miocene to the Quaternary is likely driven by the Aurora Subglacial Basin via the Vanderford Glacier. This suggests a major reorganization of ice flow from the early glaciations of the Oligocene and early Miocene to the later development of modern configurations, established in the late mid-Miocene. Our results provide the first data of the Cenozoic development of the EAIS in Vincennes Bay and demonstrate the variability of ice flow conditions with past climatic changes.

**Plain Language Summary** The long-term development of the East Antarctic Ice Sheet (EAIS) is recorded by glacially transported sediments on continental shelves. We use seismic reflection data in Vincennes Bay correlated to offshore drill sites to analyze the development of ice sheets in the region during the Cenozoic. During the Late Cretaceous to the Eocene (until ~34 Ma) fluvial channel systems shaped the continental shelf, which changed to glacial braided channel systems in the late Oligocene. Between the late Oligocene and early Miocene (~24 Ma) subglacial channel systems suggest the presence of a grounded ice sheet advancing from the western Knox Coast. From the late mid-Miocene (>~14 Ma) to the Quaternary an ice sheet likely flowed from the eastern Knox Coast, likely the Vanderford Glacier, which built up the continental shelf seawards. This suggests a change in general ice flow of the EAIS during the early Miocene to early mid-Miocene potentially due to the influence of past climatic changes.

**Key Points:**

- Alpine-like glaciers first established in Vincennes Bay during late Oligocene, replacing Late Cretaceous to Eocene rivers of alluvial plains
- Oligocene-Miocene transition tunnel valley orientation suggest early to mid-Miocene ice sheet reconfiguration to modern glacial dynamics
- Shelf progradation from late mid-Miocene to Pleistocene extends Vincennes Bay shelf through repeated glacial advances to paleo-shelf break

**Supporting Information:**

Supporting Information may be found in the online version of this article.

**Correspondence to:**

T. Mühlberger-Krause,
timo.muehlberger-krause@awi.de

**Citation:**

Mühlberger-Krause, T., Gohl, K., Hochmuth, K., Leitchenkov, G., Tobisch, C. A., Barrett, R., et al. (2026). Evolution of the East Antarctic Ice Sheet since glacial inception from seismic stratigraphic records in Vincennes Bay. *Paleoceanography and Paleoclimatology*, *41*, e2025PA005355. https://doi.org/10.1029/2025PA005355

Received 26 OCT 2025
Accepted 28 JAN 2026

**Author Contributions:**

**Conceptualization:** Timo Mühlberger-Krause, Karsten Gohl
**Data curation:** Timo Mühlberger-Krause, Karsten Gohl, German Leitchenkov, Rachel Barrett, Sebastian Krastel
**Formal analysis:** Timo Mühlberger-Krause, Chiara A. Tobisch, Rachel Barrett
**Funding acquisition:** Karsten Gohl
**Investigation:** Timo Mühlberger-Krause, Karsten Gohl, Katharina Hochmuth, Chiara A. Tobisch, Rachel Barrett, Sebastian Krastel
**Methodology:** Timo Mühlberger-Krause, Karsten Gohl



## 1. Introduction

The East Antarctic Ice Sheet (EAIS) was long presumed to remain relatively stable under current climate forcing (Stokes et al., 2022). However, recent improvements in subglacial topography data (Morlighem et al., 2020) and observations of increased ice mass loss (Stokes et al., 2022) have challenged this assumption. Vanderford Glacier drains into Vincennes Bay (Figure 1) and is the fastest retreating glacier of the EAIS, with a grounding line retreat of ~18.6 km between 1996 and 2020 (Picton et al., 2023). This glacier system experiences high rates of basal melting driven by the warmest recorded intrusion of modified Circumpolar Deep Water in East Antarctica contributing to the retreat of the EAIS in the region. Together with the Totten Glacier (Figure 1), Vanderford

**Project administration:** Karsten Gohl, Sebastian Krastel
**Resources:** Karsten Gohl, Katharina Hochmuth, German Leitchenkov, Chiara A. Tobisch, Rachel Barrett, Sebastian Krastel
**Software:** Timo Mühlberger-Krause
**Supervision:** Karsten Gohl, Katharina Hochmuth, Sebastian Krastel
**Validation:** Timo Mühlberger-Krause
**Visualization:** Timo Mühlberger-Krause
**Writing – original draft:** Timo Mühlberger-Krause
**Writing – review & editing:** Karsten Gohl, Katharina Hochmuth, German Leitchenkov, Chiara A. Tobisch, Rachel Barrett, Johann P. Klages, Sebastian Krastel

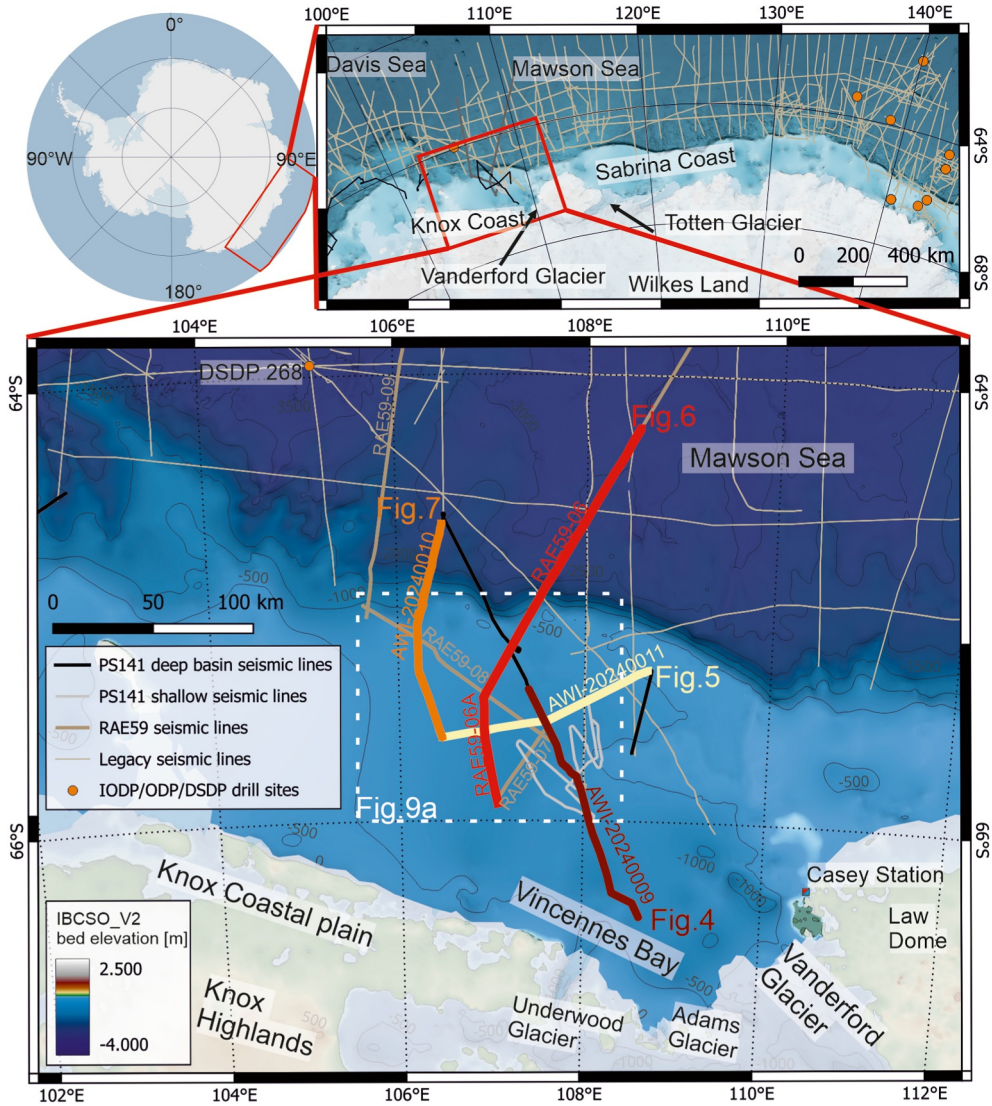


**Figure 1.** Bathymetric map with locations of multichannel seismic lines collected during expeditions PS141 (black and light-gray) and RAE59 (dark gray), DSDP, ODP, and International Oceanic Drilling Project sites (orange circles). Colored lines show locations of seismic lines shown in this study. Bathymetry from the International Bathymetric Chart of the Southern Ocean overview map, IBSCO V2 (Dorschel et al., 2022).

Glacier is a major drainage pathway of ice from the Aurora Subglacial Basin (ASB), which lies below sea-level. The ASB contains ~7 m of global sea-level equivalent (Morlighem et al., 2020), and is the most rapidly thinning basin in East Antarctica (Smith et al., 2020). Modeling studies suggest that the ASB will be the dominant contributor to sea level rise over the next tens to hundreds of years (Pelle et al., 2020, 2021). Understanding the long-term past behavior of these glacial systems is thus critical for modeling past ice sheets and future projections (Paxman, 2021).

So far, little is known about the long-term ice sheet development in Vincennes Bay, and the only indications of past ice sheet dynamics have been inferred from deep-sea sedimentary records (Hochmuth et al., 2020) and limited coverage of the continental shelf (Leitchenkov et al., 2007). New multichannel reflection seismic data collected on the Vincennes Bay continental shelf (Figure 1) provide the first insights into Cenozoic ice sheet dynamics of the Knox Coast and Vincennes Bay through analysis of glacial-marine sediments. The aim of this study is to (a) construct a seismic stratigraphic framework, (b) reconstruct the depositional environments of

Vincennes Bay during the Cenozoic and the impacts of glaciation on the continental shelf, and (c) investigate and constrain the large-scale dynamics of the EAIS since the onset of regional glaciation.

### 1.1. Geological Setting

The continental margin of Wilkes Land (~110°E–130°E) developed during the breakup of Gondwana, which separated Australia from East Antarctica creating the Australian-Antarctic Basin of the Southern Ocean. This process started with an oblique motion in the Late Jurassic during the initial opening of the Southern Ocean (Gibbons et al., 2013; Whittaker et al., 2007), but separation only occurred in the Late Cretaceous around 83 Ma (Williams et al., 2019). Slow spreading continued until 45 Ma (Williams et al., 2019) and resulted in deepening of the Tasman Rise and opening of the Tasman Gateway in the late Eocene around 33 Ma (Escutia et al., 2011; Exon et al., 2011; Scher et al., 2015). The continental margins formed in this post-rift system document the evolving oceanographic and glacial systems in the region (Hochmuth et al., 2020; Sauermilch et al., 2019). Direct records of the influence of glacial systems on this post-rift system are preserved on the continental shelves in the Davis and Mawson Sea sectors (Gulick et al., 2017; Leitchenkov et al., 2007; Montelli et al., 2020), however data coverage on the continental shelves is sparse. The Vincennes Bay continental shelf was previously interpreted as having a thin to moderate sedimentary cover (Aitken et al., 2023), with little sediment on the inner shelf and up to 10 km on the outer shelf (Leitchenkov et al., 2007). Most assumptions about the regional geology are based on examinations of pre- and syn-rift deposits on the South Australian conjugate margin and sparse geophysical observations (Close et al., 2007).

The hinterland of Vincennes Bay continental shelf is characterized by the Knox Highlands, which are dominated by Precambrian crystalline basement and separate the Vincennes Bay shelf from subglacial basins further inland (Aitken et al., 2023). The eastern region of Vincennes Bay contains glacial outlets from the extensive ASB complex within the catchment area of Vanderford Glacier and Totten Glacier with up to 5 km of sedimentary infill (Aitken et al., 2014, 2016; Young et al., 2011). The western hinterland is characterized primarily by sedimentary depocenters perpendicular to the shelf in the form of basins along the Knox Rift system (Maritati et al., 2016). The low-relief Knox Coastal plain (Eisen et al., 2020) cuts through the Knox Highlands and basement beneath the Shackleton Ice Shelf (Aitken et al., 2023), connecting Vincennes Bay shelf to Knox Basin with its 3 km thick interpreted Permian-Triassic infill (Maritati et al., 2016, 2020).

### 1.2. Glacial History

Little is known about the early glacial history of the Vincennes Bay continental shelf region due to the previously limited number of geophysical and geological data. Past ice cover in the region has been inferred from geophysical data of deep sea sediment distribution and paleo-bathymetric reconstructions along the Knox and Sabrina Coasts (Hochmuth et al., 2020). Recent modeling suggests the first coast-proximal glaciers may have reached the area from an already large hinterland EAIS during the Early Oligocene Glacial Maximum (~33.7–33.2 Ma) (Klages et al., 2024). Currently, sediment and ice discharge from Totten Glacier is higher than at Vanderford Glacier (Hochmuth et al., 2020; Li et al., 2016). This was, however, not always the case; sediment records show that sedimentation rates from Vanderford Glacier were up to twice that of Totten Glacier in the late Oligocene (27–24 Ma) (Hochmuth et al., 2020). Numerical modeling with present-day ice sheet geometries indicates a high erosive potential for the bed under both glaciers, suggesting that similar sediment discharge rates to those observed in the late Oligocene are possible (Aitken & Urosevic, 2021). Totten and Vanderford Glacier are highly dependent on each other with a transient drainage divide (McCormack et al., 2023). Numerical modeling further shows that small changes in ice sheet geometry of this system may cause substantial shifts in the distribution of ice flow between these two glaciers, influencing sedimentation rates in their respective depocenters (McCormack et al., 2023).

## 2. Data and Methods

### 2.1. Seismic Data Acquisition and Processing

The multichannel seismic data used in this study were acquired during *RV Polarstern* expedition PS141 in early 2024 (Krastel, 2025) (Figure 1). The relatively deep penetrating seismic reflection data were recorded using a 600 m long, 48 channel digital solid-state streamer (Geometrics GeoEel, on loan from NCMI-CSIRO), towed at a nominal water depth of 6 m. The data were recorded with a sampling interval of 1 ms without any recording filter.

For the seismic source, we used an array of up-to 4 GI-Guns (Sercel) with 150 $in^3$ volume each (sum of 45 $in^3$ generator and 105 $in^3$ injector volumes) towed below a steel beam in clusters of two at a nominal water depth of 2 m and operational pressure of 170 bar. Shots were fired every 10 s in True-GI mode to minimize bubble effects at a nominal ship speed of 5 knots, creating an approximate shot spacing of 25 m. Occasional issues with individual GI-Guns during seismic acquisition meant that some data were acquired using only two GI-Guns, resulting in reduced depth penetration for those sections. Furthermore, the majority of recorded seismic profiles have data gaps due to mitigation measures for marine mammal protection. We further acquired lower penetrating but higher resolution seismic reflection data on the mid-shelf of Vincennes Bay, published separately by Tobisch et al. (2025).

Over-compacted sediments at or near the seafloor cause particularly high-amplitude multiples, which is typical for continental shelves in the polar regions (Gohl et al., 2021; Hochmuth & Gohl, 2013). We found that iterative Surface Related Multiple Attenuation (SRMA) (Verschuur et al., 1992) achieved the best results for multiple attenuation and primary signal recovery for our limited offset data. SRMA was combined with move-out-based multiple suppression in the form of coherency filters, random noise suppression with shearlet filtering (Easley et al., 2008; Lim, 2010), and additional adaptive bandpass filtering to suppress remaining multiple energy. The standard seismic reflection data processing sequence included common-depth point sorting, bandpass and frequency-wavenumber (FK)-filtering, spherical divergence correction, velocity analysis, SRMA, adaptive bandpass filtering, normal move-out correction, pre-stack finite-difference migration, coherency filtering, shearlet filtering, stacking, adaptive bandpass filtering, frequency-spatial linear prediction filtering (FX-filter), and water-bottom and data gap muting. For display purposes, an automatic gain control (AGC) with a filter length of 0.5 s was applied.

We also analyzed deep-penetrating multichannel seismic reflection data acquired during Russian expedition RAE-59 in 2014, acquired using a 4,400 m long streamer with 12.5 m group spacing, and an array of 14 Sleeve Guns-IIB as a seismic source. These profiles were provided as a processed data set with standard processing applied, consisting of CDP-sorting, velocity analysis, stacking, bandpass filtering, and FX-filter. An AGC filter with a filter length of 0.5 s was also applied to these data for display purposes. Depths within seismic two-way-travel time images and thickness estimates are approximated with an average velocity of 2,250 m/s.

### 2.2. Seismic Stratigraphic Framework

Our seismic stratigraphic model of the Vincennes Bay continental shelf builds on the pre-existing stratigraphic framework of the deep sea in proximity to the study area (Donda et al., 2020; Hochmuth et al., 2020; Sauermilch et al., 2019) (Figure 2). We apply long-distance seismic horizon correlation to correlate the deep sea seismic stratigraphic models from offshore Wilkes Land (Hochmuth et al., 2020; Sauermilch et al., 2019) with Vincennes Bay continental shelf. Correlated horizons include deep-sea unconformities and key horizons WL-U1 to WL-U8 (Figure 2). Seismic stratigraphic correlation inherently includes uncertainties as a result of correlation over long distances in the deep sea, across the continental slope and onto the shelf (Gohl et al., 2021). However, a lack of nearby drill site data with continuous physical property measurements from downhole logs or core analysis, as Deep Sea Drilling Project site 268 was spot-cored, means that such a long-distance correlation currently provides the only age constraints for the proposed seismic stratigraphic units composing Vincennes Bay continental shelf. We estimate uncertainties for horizons traced from the deep sea onto the shelf to be ±150 ms on the middle continental shelf, which we determine by tracing reflector phases above and below a target horizon in the deep sea onto the continental shelf and evaluating the vertical offset to our proposed horizons on the continental shelf. Most correlation uncertainties originate on the continental slope, where units thin out significantly and multiple removal was less successful, resulting in multiples overshadowing the primary signal. Another area that introduces uncertainty is the heavily faulted transition between outer and mid-shelf.

## 3. Seismic Characterization and Horizon Stratigraphy

### 3.1. Seismic Reflection Characteristics and Features

We identify a total of eight seismic facies in our study area, based on seismic reflection characteristics, internal and external reflector geometries (Figure 3). This classification links our own observations with previous seismic facies analysis from other sectors of the Antarctic continental margin (Bart et al., 2000; De Santis et al., 2003; Escutia et al., 2003; Montelli et al., 2020; Ship et al., 1999; G. Wang et al., 2024). Further, we identified key

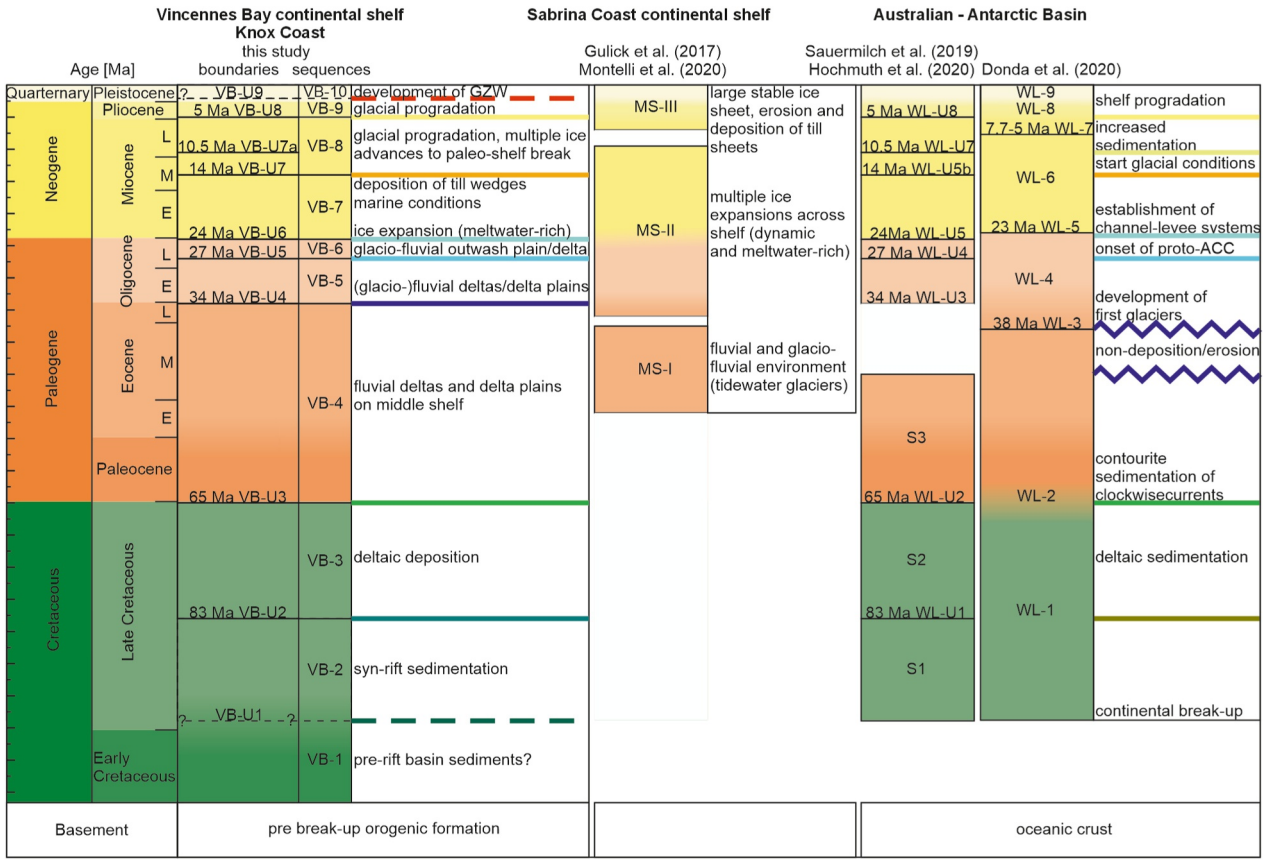


**Figure 2.** Seismic stratigraphic framework for Vincennes Bay continental shelf, compared with that of Sabrina Coast continental shelf (Gulick et al., 2017; Montelli et al., 2020) and deep-sea stratigraphy of the southern Australian-Antarctic Basin (Donda et al., 2020; Hochmuth et al., 2020; Sauermilch et al., 2019). Solid lines indicate dated boundaries correlated to the southern Australian-Antarctic Basin stratigraphy; dashed lines indicate boundaries not correlated to dated offshore stratigraphic horizon. The color scheme of sequence boundary lines corresponds to reflector horizons in Figures 4–9.

seismic features based on their geometry, facies content, and relationship to neighboring strata and secondary seismic features superimposed over seismic signatures associated with sediment deposition (Figure 3).

### 3.2. General Continental Shelf Sequence Architecture

Overall, Vincennes Bay continental shelf can be divided into a mid-shelf with well stratified shallow seaward dipping sediment strata (<~5°, Figures 4 and 5) and into an outer shelf with steeply seaward dipping prograding sediment strata (~5°–10°) truncating at the seafloor (Figures 5 and 6). The transition zone between these two regions is characterized by zones of polygonal faults crosscutting multiple sequences creating an overall chaotic character (Figures 5 and 7). Sediment thickness on the Vincennes Bay continental shelf varies between a minimum of ~9 km on the outer shelf and a minimum of ~7 km on the mid-shelf (Figure 5).

We distinguish a total of 10 sequences (VB-1 to VB-10, Figure 2) bounded by top unconformities VB-U1 to VB-U9 and the seafloor on the continental shelf. These sequences are grouped into syn-rift, post-rift pre-glacial, post-rift glacial transition, and post-rift-glacial seismic units. The key shelf sequence boundaries are determined through correlation via two independent correlation paths to the deep-sea seismic records offshore Wilkes Land (Hochmuth et al., 2020; Sauermilch et al., 2019) and are self-consistent on the continental shelf. These sequence boundaries represent basin-wide events within the Australian-Antarctic deep-sea basin cross-referenced with multiple International Oceanic Drilling Project drill sites and provide the best estimates for ages of stratigraphic units. Additional sequences are defined by dominant seismic facies changes (Figure 3) and regional unconformities (Figure 2). Age estimates of these are based on stratigraphic context and comparison to other regions of the East Antarctic margin and have a higher level of uncertainty. We further define subsequences separated by

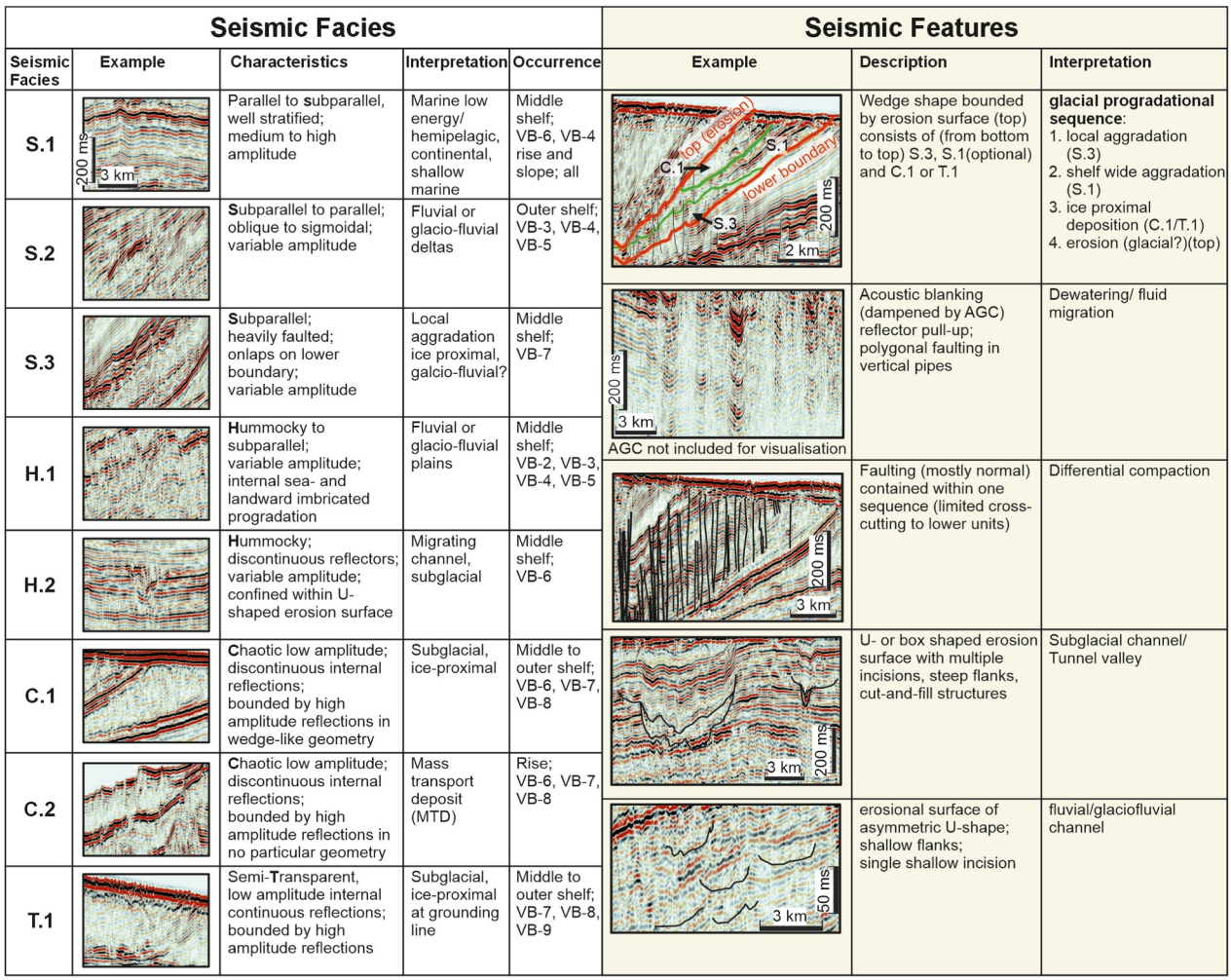


**Figure 3.** Major seismic facies and seismic features identified from seismic records of the continental shelf in Vincennes Bay. The scale of the seismic images is consistent for the seismic facies column.

corresponding subsequence boundaries (i.e., VB-U6.2 within VB-7) representing unconformities or changes in seismic facies within sequences, if so specified, adding a process-based framework to the stratigraphic age model.

### 3.2.1. Syn-Rift Unit

*VB-1* (top: VB-U1) is characterized by well stratified, parallel to sub-parallel reflectors, typical of facies S.1, interlayered with transparent to low-amplitude transparent layers found on the mid-shelf (Figure 4) and in the deepest imaged shelf region (Figure 5). Northward-dipping normal faults within this sequence are separated from upper sequences by an angular discordance with a rough surface VB-U1 which is interpreted as the breakup unconformity in the mid-Cretaceous (between ~100 and 83 Ma).

*VB-2* (top: VB-U2 ~83 Ma, WL-U1; Hochmuth et al., 2020; Sauermilch et al., 2019) consists of facies S.1 and S.2 with steep north-dipping normal faulting crosscutting through lower units into VB-2 (Figure 5). The overall thickness of VB-2 increases toward distal environments, and is thinnest at the modern transition between outer and mid-shelf (Figure 5).

### 3.2.2. Post-Rift-Preglacial Unit

*VB-3* (top: VB-U3 ~65 Ma, WL-U2; Hochmuth et al., 2020; Sauermilch et al., 2019) is composed of mostly parallel to subparallel seismic facies S.1 on the mid-shelf, while VB-3 on the modern outer shelf is dominated by

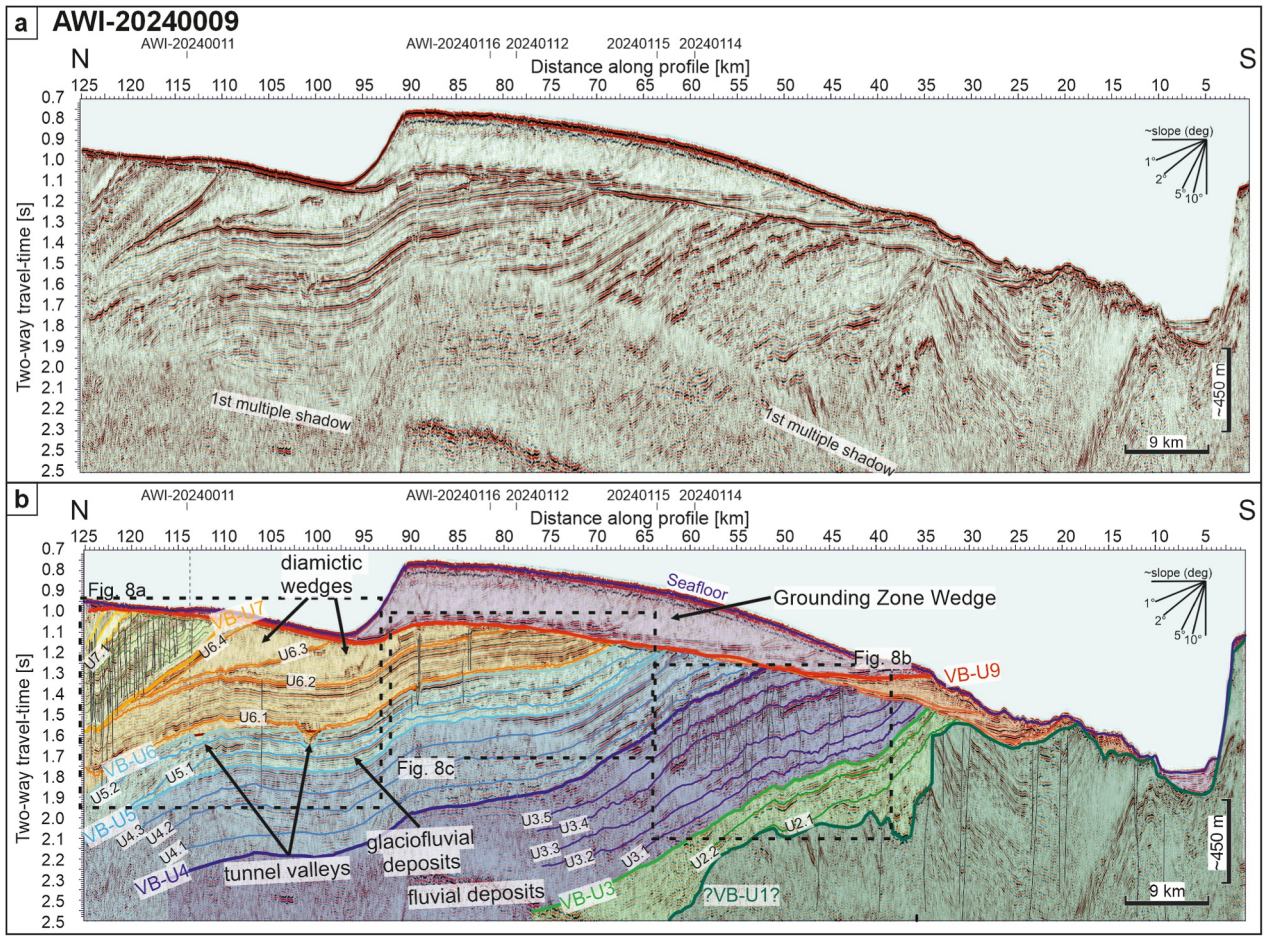


**Figure 4.** Seismic reflection profile AWI-20240009 on the mid continental shelf. (a) Processed seismic section with multiple suppression. (b) Interpretation of the main seismic stratigraphic sequences, subsequences, and sedimentary features. Location of the profile is shown in Figure 1.

progradational patterns of S.2. The overall thickness of VB-2 increases significantly from the modern mid-shelf to the modern continental rise. Small scale progradational patterns are imaged within subsequences in the most shelf-proximal data collected (Figures 4 and 8b).

*VB-4* (top: VB-U4 ~34 Ma, WL-U3; Hochmuth et al., 2020; Sauermilch et al., 2019) is composed of a series of subparallel to rugged high amplitude reflectors representing the tops of subsequences of facies H.1. on the modern mid-shelf. Further seaward the sequences change to subparallel units of facies S.2, exhibiting larger progradational patterns (Figure 5). On the modern outer shelf, these sequences thin toward the continental slope and rise to subparallel layers of facies S.1.

### 3.2.3. Post-Rift Glacial Transition Unit

*VB-5* (top: VB-U5 ~27 Ma, WL-U4; Hochmuth et al., 2020) is characterized by stratified thick (~500 ms) layers of facies S.1 in the modern mid-shelf area (Figures 4 and 8a), topped by shallow angular unconformity VB-U5. These stratified layers change into oblique and sigmoidal progradational patterns characteristic of facies S2.1 on the modern outer shelf (Figure 5). Lower subsequences of VB-5 exhibit a reflection character characteristic of facies H.1 in the most landward section (Figure 4).

*VB-6* (top: VB-U6 ~24 Ma, WL-U5; Hochmuth et al., 2020) is composed of subsequences characterized by facies S.1 on the modern mid-shelf, with single reflectors interrupted by small-scale imbricated progradational patterns and shallow channelized incisions (Figure 4). Further seaward, these sequences transition to sub-parallel reflectors in progradational sigmoidal to oblique patterns as in facies S.2 (Figure 6) and semi-transparent mounded

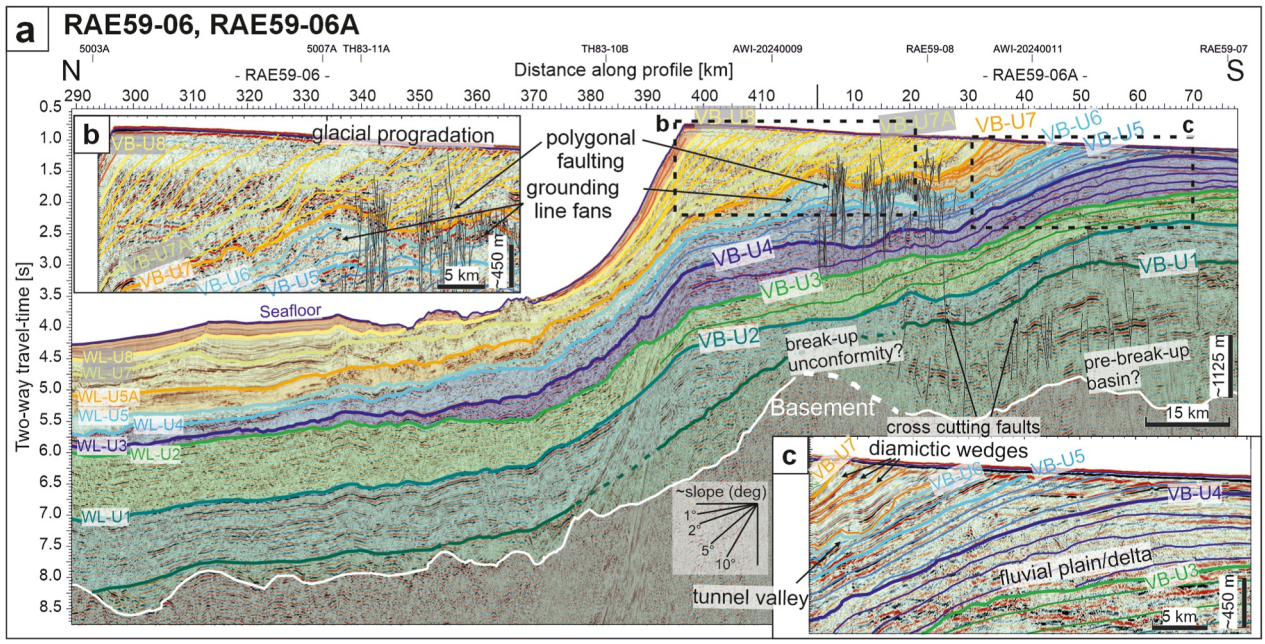


**Figure 5.** (a) Seismic reflection profiles RAE59-06 and RAE59-06A with interpretation of the main seismic sequences, subsequences, and sedimentary features illustrating the general shelf architecture. (b) Steeply prograding outer shelf and (c) shallow dipping mid-shelf sequences. Location of the profile is shown in Figure 1. An uninterpreted version of this seismic section is shown in Figure S1 in Supporting Information S1.

features (Figure 5). VB-U6 exhibits multiple channelized incisions across the modern mid-shelf, ranging from 0.6 to 8 km in horizontal cross-sectional extent and 30–120 ms (Figures 4, 5, 7, and 8a).

### 3.2.4. Post-Rift Glacial Unit

*VB-7* (top: VB-U7 ~14 Ma, WL-U5b; Hochmuth et al., 2020) is immediately overlying the erosional unconformity VB-U6 (~24 Ma) with its channelized incisions (Figures 4 and 7), and the lowermost units of VB-7 are composed of facies H.2, which fill these channels. These channel in-filling lowermost units of VB-7 also show indications of channelized incisions, often in the same place as channels along VB-U6 (Figures 4 and 7). This unconformity is overlain by 200 ms thick layers of facies S.1 stretching over the entire mid-shelf (Figure 4). In the modern mid-shelf, the upper subsequences of VB-7 consist of three distinct low amplitude wedge-like units of facies C.1 separated by high amplitude reflectors (U6.2–U6.3), merging with the top boundary VB-U7 toward the outer shelf (Figures 4, 6, and 8a).

*VB-8* (top: VB-U8 ~5 Ma, WL-U8; Hochmuth et al., 2020) is characterized by steeply dipping (~5°–10°) prograding subsequences with an overall trend of seaward increasing slope angle toward modern shelf break. These subsequences consist of a lower subparallel facies S.3 onlapping on the lower boundary, a middle facies of subparallel facies S.2 and an upper wedge-like section of facies C.1 or T.1 (Figure 3). The lower and middle facies are often crosscut by polygonal faults and vertical acoustic blanking combined with reflector pull-up. The tops of these subsequences are erosional unconformities that truncate the downlaps of lower facies (Figures 3 and 6c). Only limited examples of these subsequences with topsets are preserved due to erosional unconformity VB-U9 on the outer shelf. We identify at least 27 such subsequences within VB-8, with maximum thickness varying widely across subsequences for all facies (50–200 ms). However, data gaps make a continuous interpretation of subsequences impossible. VB-8 also includes the boundary VB-U7A (10.5 Ma, WL-U7; Hochmuth et al., 2020) after which there is an increased occurrence of layers of facies C.1 on the continental rise.

*VB-9* (top: VB-U9, <5 Ma) is composed of the same subsequences as VB-8 (Figures 3 and 6c), with thinner or missing wedges of facies C.1, compared to subsequences of VB-8. Slump scars are visible on the modern shelf break (Figure 6). The top of VB-9, VB-U9, is estimated to be of Quaternary age and coincides with the seafloor on the seismic scale on the outer shelf and parts of the mid-shelf. Within VB-9 we include the most proximal wedge characterized by facies S.1 since its top boundary is VB-U9 and lies on an unconformity to VB-4, VB-5, and VB-6

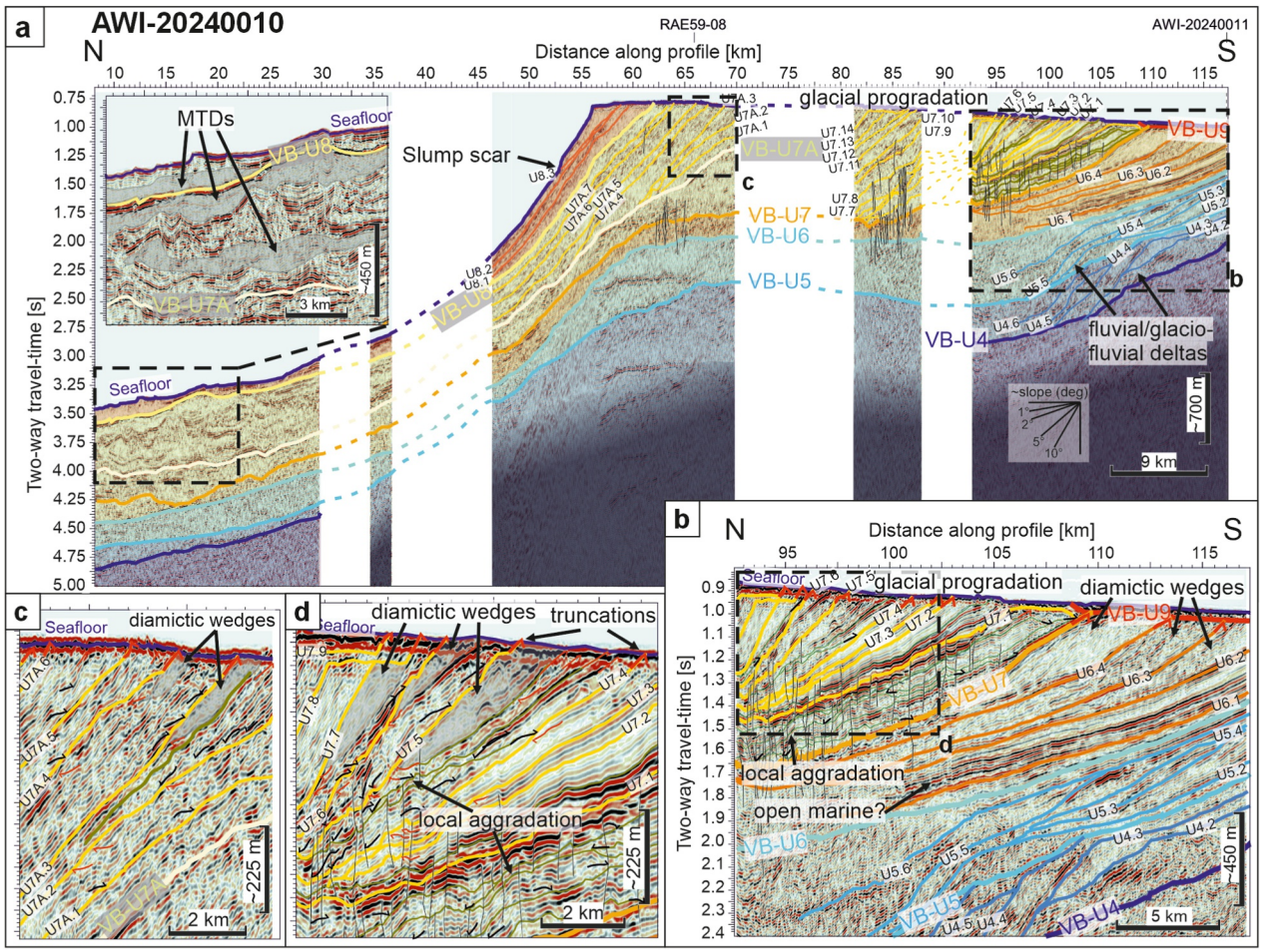


**Figure 6.** Seismic reflection profile AWI-20240010. (a) Interpretation of the main seismic sequences, subsequences, and sedimentary features. (b) Prograding sequences on mid-shelf resulting from fluvial and glacial processes. Glacial progradation on the (c) outer shelf in late mid-Miocene and (d) mid-shelf in the late Miocene. Location of the profile is shown in Figure 1. An uninterpreted version of this seismic section is shown in Figure S2 in Supporting Information S1.

(45–20 km, Figure 4). It is important to note that no meaningful age correlation could be achieved and these sediments within VB-9 could have been deposited during the deposition of VB-6–VB-9.

*VB-10* is characterized by a massive (~250 m thick) semi-transparent section of facies T.1 with a wedge-like configuration with a steep wedge flank on its distal side and low amplitude internal foreset features (Figure 4). This wedge is deposited in the eastern mid-shelf proximal to the glacial outlet of Vanderford Glacier. Only thin sediment layers often below seismic resolution are deposited seaward of the steep flank.

## 4. Depositional Environments

### 4.1. Cretaceous-Paleogene Fluvial Systems

Seismic sequences VB-1 (top VB-U1) to VB-4 (top VB-U4 ~34 Ma) exhibit no stratigraphic evidence of glacial erosion or deposition, suggesting that no major grounding line advance onto the continental shelf occurred until the end of the Eocene (~34 Ma, VB-U4). The overall seismic character (facies H.1) of mid-shelf subsequences of VB-4 and distal delta structures (Figures 5 and 6) are likely associated with fluvial deposition (Y. Wang et al., 2021). Within VB-4 and partly also VB-3 (VB-U3, ~65 Ma) small-scale imbricated progradational patterns (~2 km wide and ~50 ms thick) contained within channelized incisions break the reflector continuity of relatively stratified sections on the mid-shelf (Figures 4 and 8b). These structures are characteristic of laterally migrating channel systems found throughout lower latitude settings (Abreu et al., 2003; Jobe et al., 2016), where they represent fluvial systems. This suggests an extensive network of Late Cretaceous–Eocene channel systems and

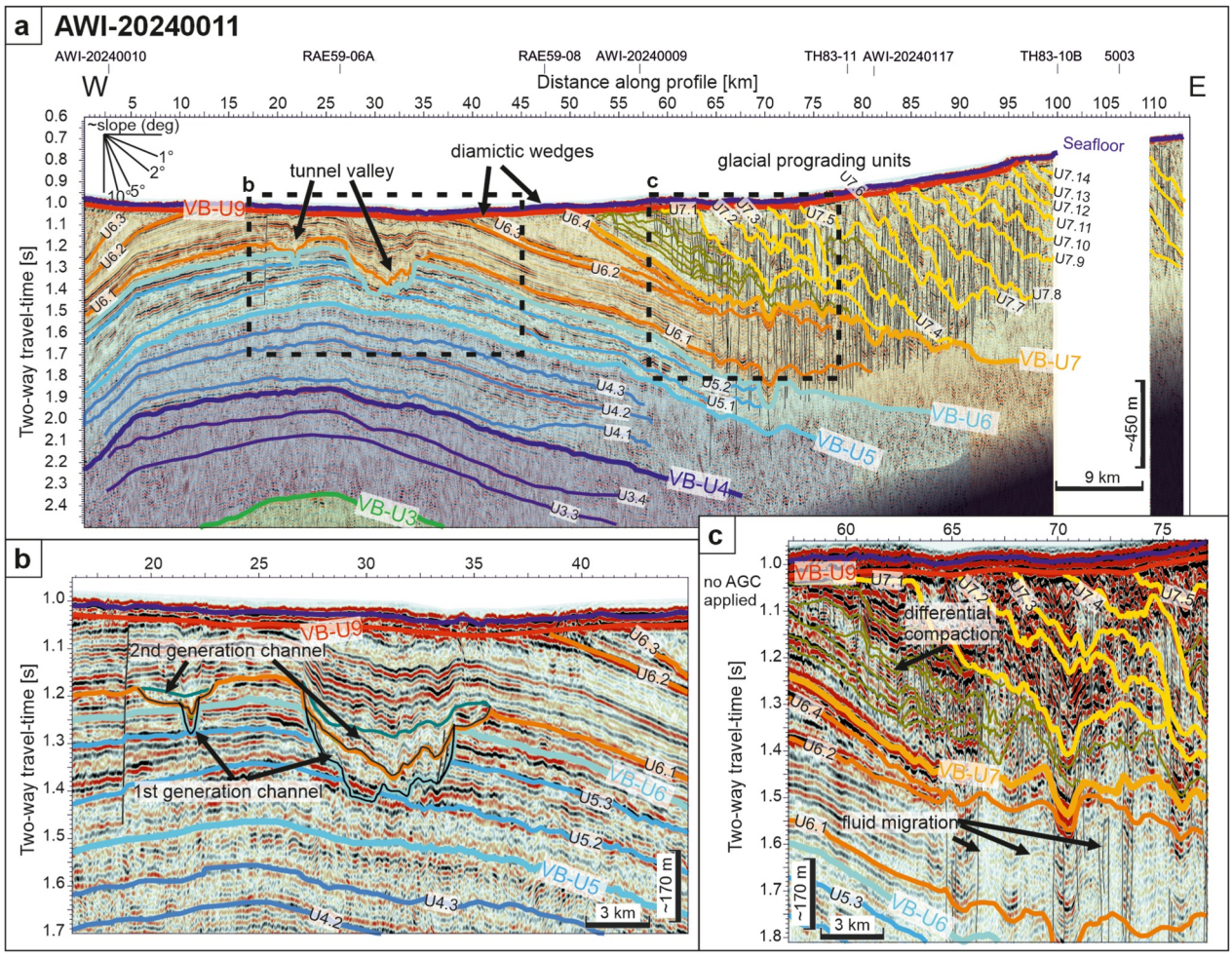


**Figure 7.** Seismic reflection profile AWI-20240011. (a) Interpretation of the main seismic sequences, subsequences, and sedimentary features. Only 2 airguns were active during acquisition of AWI-20240011. (b) Largest observed subglacial U-channel cross-section with reactivated surfaces. (c) Inset showing glacial progradation, differential compaction, faulting and fluid migration zones. No automatic gain control applied in panel (c) so that lateral amplitude variations are clear and fluid migration is visible. Location of the profile is shown in Figure 1. An uninterpreted version of this seismic section is shown in Figure S3 in Supporting Information S1.

deltaic environment in Vincennes Bay. Presence or absence of a potential distal glacial source further inland during late Eocene deposition cannot be resolved by our data set. However, there is no sign of ice proximal to Vincennes Bay and therefore we suggest a mainly fluvial deposition. Other channelized features with a hummocky character have recently been related to braided river deposition in an Eocene West Antarctic delta environment (Zundel et al., 2024).

### 4.2. Glaciofluvial Outwash Plains

Within subparallel reflection patterns of VB-6 (top VB-U6 ~24 Ma), imbricated prograding foresets interrupting single reflectors indicate small scale prograding deltas associated with systems of braided river channels (Dong et al., 2015). These, and landward shallow incisions into the same reflector (Figures 8a and 8c), suggest the presence of shallower braided channel systems (Figure 8d). Similar deposits in the Barents Sea in the northern hemisphere have been described as glacio-fluvial outwash plains characterized by glacial outburst flooding (Bellwald et al., 2021), which suggests the presence of small glaciofluvial systems in front of glacial outlets in a coastal environment during the deposition of VB-6. This indicates the presence of grounded ice in the direct vicinity of Vincennes Bay. Even more distally, these deposits change to larger scale delta structures of facies S.2 (Figure 8a) indicating the maximum seaward extent of the buried outwash plains present between ~27 and ~24 Ma.

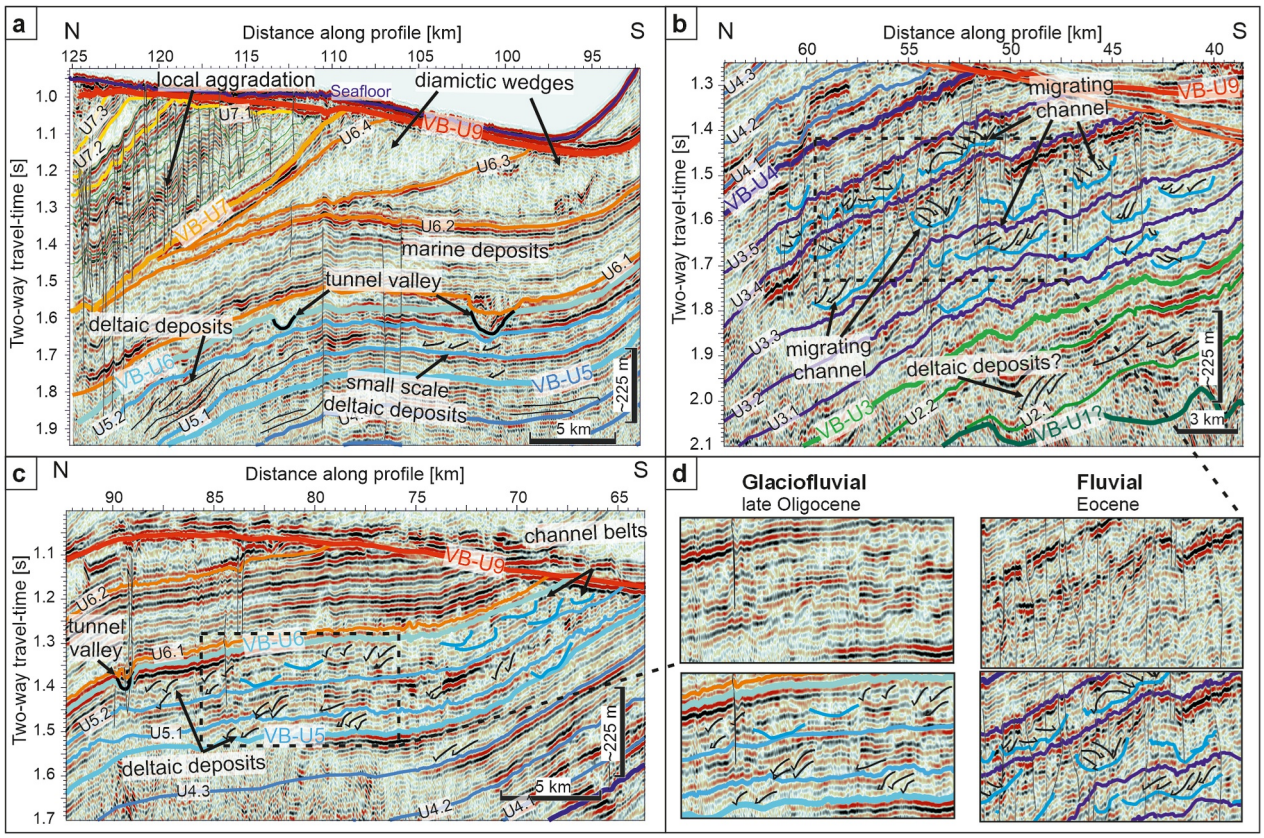


**Figure 8.** (a) Glacial features on the mid-shelf: tunnel valleys, diamictic wedges and local aggradation, and glaciofluvial deltaic deposits and small-scale prograding deltas. (b) Paleogene and Eocene-Paleogene channel systems in AWI-20240009. (c) Glaciofluvial outwash plains, small-scale prograding delta and channels. (d) Comparison between glaciofluvial and fluvial channels and small-scale deltas. Zoomed sections (a–c) of AWI-20240009 outlined in Figure 4.

The deposits of VB-5 (top VB-U5 ~27 Ma) exhibit only limited imbricated progradational delta patterns often associated to braided channels (Dong et al., 2015; Zundel et al., 2024) in its upper most subsequence VB-4.4 (Figure 8c). Lower subsequences (4.3, 4.2, and 4.1) consist mostly of facies S.2 with limited evidence of channelized incisions into single reflectors (Figure 8c) and larger deltaic structures on the outer shelf (Figure 6a). This suggests a transitionary period from the earlier migrating channel systems in VB-4 (~65 to ~34 Ma) to the later observed glaciofluvial outwash deposits in VB-6 (~27 to ~24 Ma), where a likely ice-distal environment transitions to ice-proximal glaciofluvial due to ice expansion in the hinterland.

### 4.3. First Major Ice Sheet Advance Onto the Continental Shelf

Channelized features along discontinuities VB-U6 (~24 Ma) and VB-U6.1 are spread across the imaged mid-shelf (Figures 4, 5, and 7). These channels cut into underlying sequences, have steep flanks, and flat or multiply incised channel beds, (Figures 9b–9e) and can therefore be classified as buried tunnel valleys suggesting subglacial formation (Kehew et al., 2012). It is difficult to determine the absolute channel width from limited 2D cross sections at irregular angles. However, the channels imaged in our data seem to have a wide range of apparent width from ~1 to ~11 km and depth from ~50 ms (~60 m) to ~260 ms (~290 m). The largest channel was imaged across three seismic lines, giving a rough estimate of ~6 km for the channel width (Figure 9a). These are similar morphometric properties to other tunnel valleys in the northern and southern hemispheres (Berger et al., 2008; Kristensen et al., 2008; Lonergan et al., 2006; Montelli et al., 2020; Stewart et al., 2013). Bed topography data in the modern Vanderford Glacier outlet shows similar geometry and channel size in its meltwater landforms (McCormack et al., 2023).

Almost all channels exhibit an asymmetric configuration with one steeper flank (Figures 9b, 9d, and 9e). This morphology is consistent with the complex anastomosing character often observed in subglacial meltwater

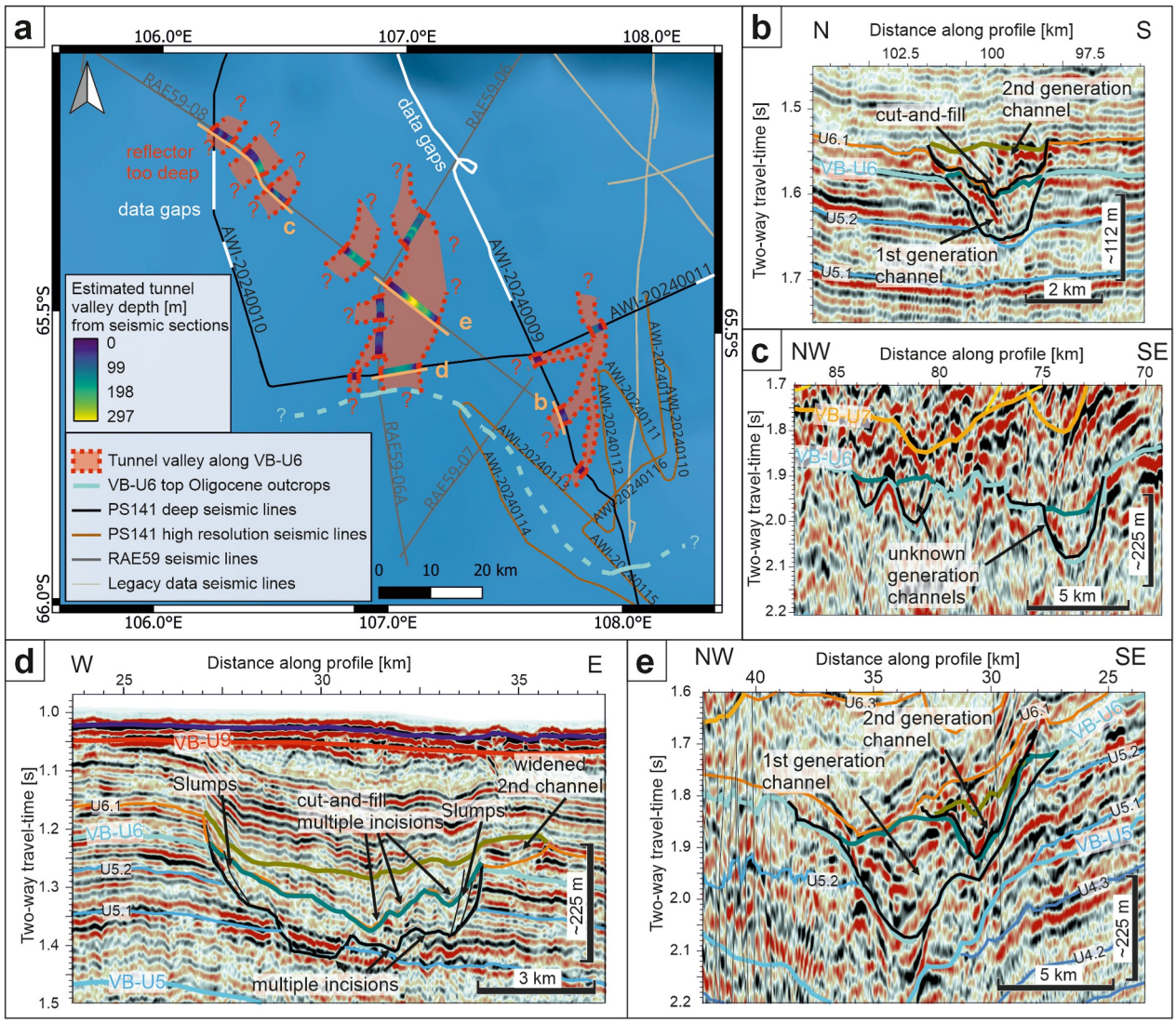


**Figure 9.** Tunnel valleys along VB-U6: (a) Map of interpreted channel extent, flanks, and estimated channel depth for mapped tunnel valley cross-sections along VB-U6 with the interpreted tunnel valley pathways and seafloor-truncations of VB-U6. Location of zoomed map view in Figure 1. (b) Cross-section of eastern channel system in AWI-20240009. (c) Cross-sections of channels of western channel system in RAE59-08. Cross-sections of largest tunnel valley in (d) AWI-20240011 and (e) RAE59-08 showing multiple incisions, slumping, and reactivation.

channel systems (Bellwald et al., 2024; Kirkham et al., 2024; Lohrberg et al., 2020; Lonergan et al., 2006; Montelli et al., 2020). The flanks of the largest channel imaged in our data exhibit slumping (Figure 9d), which has been suggested to be triggered by ice removal destabilizing channel flanks (Kirkham et al., 2024). Cut-and-fill structures along VB-U6.1 with multiple incisions into the lower fill sediments within the mid- and larger-sized channels (Figure 9) indicate a reactivation and second generation of tunnel valleys (Jørgensen & Sander-sen, 2006). Widening at the top of the tunnel valley along VB-U6.1 (Figure 9d) indicates lateral migration (Stewart et al., 2013) of subglacial water flow of the second-generation channel. This suggests a glacial retreat after initial tunnel valley formation, and the reactivation of tunnel valleys in a subsequent grounding line advance.

We used the seismic characteristics of the tunnel valleys (channel bends, cross-sectional area, and their presence or absence in cross-sections) to reconstruct the direction and connectivity of the first generation of tunnel valleys (Figure 9a). The orientation and spatial distribution of the imaged subglacial channel cross-sections suggest the existence of three channel systems with a general NE-SW orientation (Figure 9a). However, data coverage is sparse at best, and determining channel generation in the lower-resolution RAE seismic data is impossible unless an obvious reactivation or crosscutting is observed (Figures 9c and 9d). Smaller channels are likely below the data

10.1029/2025PA005355

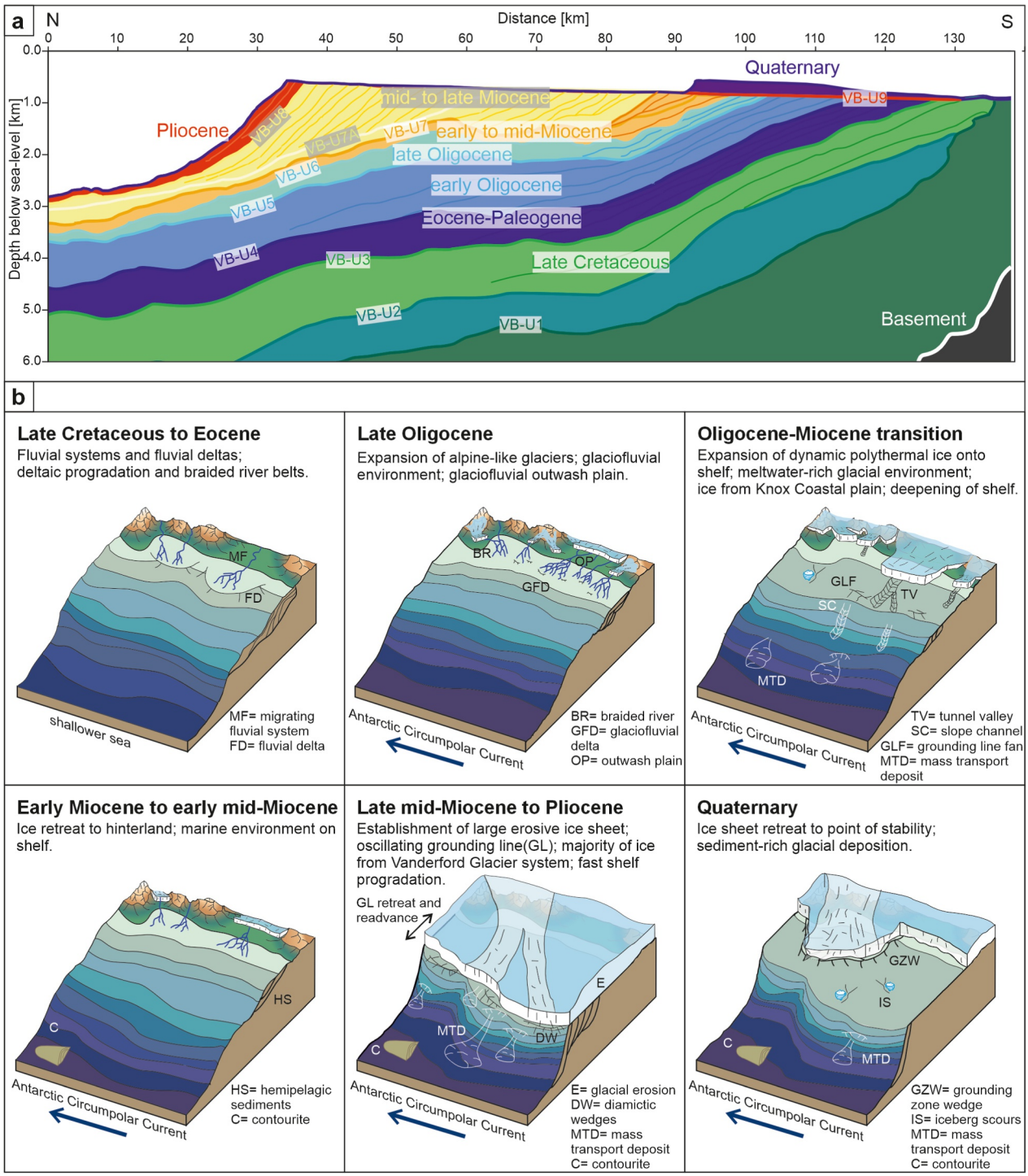


**Figure 10.** (a) Geological section across the eastern Vincennes Bay continental shelf derived from seismic reflection data. (b) Proposed depositional environments and grounded ice expansions on the Vincennes Bay continental shelf through time with observed and interpreted depositional features. Deep-sea evolution based on Hochmuth et al. (2020) and Sauermilch et al. (2019).

resolution and therefore not identifiable. The central channel system is the largest, and the eastern system exhibits the smallest width and erosion depth. No further channels were imaged farther west in the PS141 shallow high-resolution data set (see data of Tobisch et al. (2025)) and legacy data. The general subglacial water flow direction follows the hydraulic gradient underneath ice sheets which, in combination with hydrological subsurface

properties, controls the channel direction (Jørgensen & Sandersen, 2006; Kehew et al., 2012). This suggests a paleo-hydraulic potential decreasing from SW to NE, potentially indicating a paleo-ice flow direction in the same direction during the time of tunnel valley formation.

More distal mounded semi-transparent features within VB-6 close to the modern shelf break (Figure 5) resemble grounding line fans formed at the front of meltwater-rich glaciers (Leitchenkov et al., 2015; McKay et al., 2022; Powell & Cooper, 2003). At least two of these are present on the continental shelf directly below VB-U6 and likely associated with the tunnel valleys of VB-U6 and VB-U6.1, suggesting at least two successive extensive polythermal ice expansions on the continental shelf around ∼24 Ma. This would mark the first establishment of a grounded marine based polythermal ice sheet on the Vincennes Bay continental shelf, where the ice sheet was in contact with its bed below sea level.

Following the second phase of tunnel valley formation, a well stratified subsequence VB-6.2 (200 ms/∼225 m thick) was deposited, indicating a transition to a marine depositional environment. This lacks any indications for grounded ice, suggesting a grounding line retreat farther inland for most of the early Miocene to early mid-Miocene. However, the absolute degree of glacial influence and ice proximity during this time remains uncertain due to the ambiguity of interpreting seismic reflection characteristics, as demonstrated by the drilling of similar well-stratified seismic units in the Ross Sea revealing layered diamictites with variable clast content (McKay et al., 2024).

### 4.4. Shelf-Wide Grounding Line Advances

The three seismically chaotic wedges of VB-7 (Figures 4–7) with steep seaward flanks suggest a fast deposition with a steep gradient in transportation energy. Similar internally chaotic (facies C.1), wedges with similar boundary geometries are found on the continental shelf in the Ross Sea and interpreted as diamictic wedges formed by subglacial, glacio-marine, and gravity flow deposits (G. Wang et al., 2024), which are deposited by the release of eroded sediments at the grounding line (Bart, 2003; Bart et al., 2000). The shelf-wide distribution of these diamictic wedges over the entire imaged continental shelf suggests the presence of an expansive grounded ice sheet covering the continental shelf during their deposition.

The sediment that constitutes the diamictic wedges was eroded and transported by three consecutive grounding line advances, before being deposited on the deepened continental shelf further proximal than previous glacial advances (Figure 5). Deposition of these diamictic wedges markedly steepened the continental slope, changing dips from <∼4°, in older sequences VB-2 to VB-6, to ∼5°–7° in the upper parts of VB-7, VB-8, and VB-9 (dips as observed on modern configuration) (Figures 5 and 6). This process created a northward progression of the shelf break indicated by later progradation starting from the wedge deposits. The thickness of the lower two diamictic wedges (VB-6.3 and 6.4) decreases from ∼200 ms (∼225 m) in the west (Figure 6) to ∼100 ms (∼110 m) in the east (Figure 4) indicating more sediment supply from the direction of the Vanderford Glacier.

### 4.5. Glacially Induced Shelf Progradation

We observe a minimum of 30 progradational seismic units (Figure 3) on the steeply dipping (∼5°–10°) outer shelf in VB-8 (minimum 27 units) and VB-9 (3 units) (Figures 5 and 6). None of these units have preserved topset sediment, and reflectors are truncated at or close to the seafloor. These truncations indicate the presence of grounded ice, which eroded the tops of dipping strata. Similar outer shelf truncations have been observed in the Ross Sea (Bart, 2003; De Santis, 1999; G. Wang et al., 2024) and Prydz Bay (Cooper et al., 1991; O'Brien et al., 2004), where they are associated with glacial diamicts (Cooper et al., 1991).

The topmost facies within these progradational units (T.1 and C.1) are associated with ice-proximal deposition (Gulick et al., 2017; Montelli et al., 2020; G. Wang et al., 2024), indicating the presence of a grounded ice sheet close to the paleo-shelf break. The top discontinuity of prograding subsequences is interpreted as representing downslope erosion due to gravity flows during the maximum glacial extent. Some later unconformities (after VB-U7A) are associated with an increased occurrence of mass transport deposits (MTDs) on the continental rise (Figure 6a). Increased occurrence of MTDs has also been linked to ice sheet expansion dynamics on steep continental slopes (>5°), which initiate upper slope failures (G. Wang et al., 2024). Thus, an extensive grounded ice sheet that caused seaward migration of the shelf break and steepening of the continental slope would explain the increased occurrence of MTDs on the continental rise.

The lowermost facies (S.3) of the progradational subsequences has varying thickness and forms onlap-structures (Figure 6). This indicates local aggradation along the entire paleo-shelf break and suggests either a lack of accommodation space further landward or significantly higher deposition rates on these slopes. Glacially dominated shelves on the East Antarctic margin were deeper (Paxman et al., 2019) than the expected amplitude of sea-level fluctuations and are unlikely to have caused the minimal deposition on the continental shelf and distal aggradation. Previous studies have suggested that grounded ice sheets deposit marine outwash muds directly in front of morainal banks close to the grounding line (Powell & Cooper, 2003), and if extended to the paleo-shelf break, deposit these outwash muds downslope as sediment gravity flows (Bart, 2003). Given a sufficiently steep slope >~5°, we suggest these tend to settle further downslope and form aggrading depositional patterns.

Based on observations on other high latitude continental margins (Cooper et al., 1991; Gohl et al., 2013), we infer that reflectors of facies S.1 truncating at the seafloor were widespread over the entire or at least parts of the paleo-shelf suggesting shelf-wide aggradation. This implies the shelf-wide filling of accommodation space. Thus, facies S.1 is interpreted as representing a period of grounding line retreat farther inland (Figure 3). The lack of topset sediments across the entire imaged outer continental shelf, coupled with the presence of ice-proximal facies within most prograding subsequences, implies that deposited topset sediments were eroded during repeated ice advances. This indicates that topset sediment deposition on the continental shelf during periods of glacial retreat was insufficient to enable preservation during subsequent erosive grounding line advances. Therefore, we propose that progradational units were mainly formed during glacial cycles with grounding line advances to the paleo-shelf break. Another possibility is that one, or a few, extremely erosive glacial advance(s) could have caused this level of erosion, similar to that observed in the Ross Sea (Bart, 2003). The combination of frequent occurrence of inferred ice-proximal deposits, steep dips and a high number of prograding subsequences with these features suggests highly dynamic ice-sheet behavior during deposition of VB-8 and VB-9, making multiple ice sheet advances with reoccurring erosion more likely.

### 4.6. Late Glacial Dynamics

The erosional discontinuity near the seafloor (VB-U9) extends across the entire imaged continental shelf, truncating reflectors of sequences VB-2 to VB-9 up to the modern shelf break (Figures 5 and 6). The association of erosional discontinuities with grounded ice sheets (Bart, 2003; De Santis et al., 2003) and thin sediment cover suggests an extensive grounded ice sheet must have existed within the Pliocene and Quaternary. On the mid-shelf, a wedge-like deposit with a steep, prograding distal flank is interpreted as a grounding zone wedge (GZW) by Tobisch et al. (2025) (shown in Figure 4). GZWs from recent glacial retreats have been observed on many high-latitude continental margins (Batchelor & Dowdeswell, 2015; Batchelor et al., 2014; Fernandez et al., 2018; Guitard et al., 2016; Klages et al., 2017), as well as preserved, buried ones (Gohl et al., 2021). A detailed discussion of this GZW is beyond the scope of this paper and will be discussed elsewhere. For our purposes, this GZW indicates a period of stable grounding line extent (Batchelor & Dowdeswell, 2015) during retreat from the shelf break and likely deposited during the Quaternary.

### 4.7. Glacial Load Induced Structures

The presence of faults limited in stratigraphic extent to single subsequences in VB-8 (Figures 5, 7, and 8a) suggests differential compaction due to the addition of a heavy load onto poorly compacted sediment (Grollimund & Zoback, 2000; Landschulze & Landschulze, 2021). Such loading may occur during the advance of grounded ice sheets onto poorly compacted sediment. The presence of polygonal faulting, acoustic blanking and reflector pull-up structures (Figure 6c) indicates pathways of fluid migration (Weigelt et al., 2012). These features are observed throughout the outer continental shelf in Vincennes Bay and indicate fluid migration from deep, oversaturated sequences (VB-6 and VB-5) to the surface, suggesting dewatering due to increased glacial load.

## 5. Discussion: The Evolution of the EAIS in Vincennes Bay

### 5.1. Pre-Glacial Fluvial Plains

The absence of seismic features associated with glaciations, together with the presence of fluvial plain and delta deposits up to VB-5 (Figures 8a and 8c), suggests that there was no glacial influence on the continental shelf until the late Oligocene. Buried migrating channel sediment structures within the Late Cretaceous (VB-3), Paleocene and Eocene (VB-4), and lower early Oligocene (VB-5) sequences suggest an ice-free, coastal, alluvial plain

setting in Vincennes Bay (Figure 10). Fluvial landforms between 34 and 14 Ma (and potentially older) have been identified further inland in the Vanderford Glacial Trough in the ASB (Jamieson et al., 2023), and have been postulated for this region before the onset of glaciation (likely before 34 Ma) with a flow direction from the Knox Coastal plains (Paxman et al., 2025). Our data suggests that fluvial systems along the Knox Coast influenced Vincennes Bay from the Late Cretaceous until the Eocene (~34 Ma) and slowly disappeared in the early Oligocene.

### 5.2. Establishment of Alpine-Like Glaciers and Outwash Plains

Late Oligocene and partially upper early Oligocene deposits show evidence of glaciofluvial outwash plains on the proximal shelf (Figures 8a and 8c). This suggests the presence of oscillating grounded coastal ice in a terrestrial to coastal setting between ~27 and 24 Ma. These outwash plain deposits are the earliest evidence of grounded ice in the vicinity of Vincennes Bay continental shelf. A similar setting of alluvial plains, deltas or glacial outwash has been observed in Prydz Bay during the late Eocene (Erohina et al., 2004; Passchier et al., 2017), where first indications of alpine glaciers were observed in the late Eocene (Passchier et al., 2017). The first evidence of a continental scale ice sheet exists in the Ross Sea, where the first signs of grounded ice date to the early Oligocene ~32.8 Ma (Galeotti et al., 2016), and the Sabrina Coast, where first glacial advances and the development of tunnel valleys occur during the late Eocene and Oligocene (Gulick et al., 2017; Montelli et al., 2020). In contrast, our data indicate a mostly terrestrial ice sheet with alpine-like to tidewater glaciers in Vincennes Bay during the Oligocene, which only reached the proximal continental shelf in coastal regions in the late Oligocene (Figure 10). This suggests that ice cover established later in the vicinity of Vincennes Bay continental shelf than around other sectors of the East Antarctic margin (Klages et al., 2024), potentially indicating a smaller EAIS that did not reach the Vincennes Bay area until later in the early Oligocene.

### 5.3. Meltwater-Rich Glaciations and Their Retreat

Around 24 Ma, likely during the Oligocene-Miocene Transition, meltwater-rich glaciations extended onto the continental shelf, creating subglacial channel systems with an inferred NE-SW trend (Figures 9 and 10). Since subglacial channels follow the hydraulic gradient, the channel direction indicates the general ice thickness gradient (Jørgensen & Sandersen, 2006; Kehew et al., 2012). We interpret that the inferred direction of these tunnel valleys, and their absence in data collected on the eastern shelf, indicates polythermal grounded ice advances from Knox Coast onto the continental shelf, rather than from the modern main glacial outlets of Vanderford and Adams Glaciers. The reactivation of these tunnel valleys indicates multiple ice advances of a highly dynamic polythermal ice sheet with a preferred ice flow direction from the Knox Coastal plain to NE (Figure 9a). This suggests that early ice advances in this area were driven by glacial outlets of the Knox Highlands (Figure 1), or through the Knox Coastal plain from Knox Basin or Queen Mary Land, rather than by modern main glacial outlets of the ASB in Vincennes Bay (Vanderford, Underwood, and Adams Glaciers). We suggest that the high sedimentation rate observed in the deep sea offshore Knox Coast in the late Oligocene (27–24 Ma) (Hochmuth et al., 2020) may have been significantly influenced by these paleo-glacial outlets.

This behavior differs from the nearby Sabrina Coast, where tunnel valleys developed over a longer time span from the Late Eocene to Late Miocene and five separate glaciations (Gulick et al., 2017; Montelli et al., 2020). In contrast, tunnel valley development in Vincennes Bay initiated later during the Oligocene-Miocene Transition and was limited in time to two subsequent glaciations. This suggests regional differences in the timing of ice sheet development between these neighboring glacier systems, which are linked in the modern ice sheet configuration.

The part of our study area most proximal to the coast transitioned from a coastal or terrestrial environment during the late Oligocene (~27 to ~24 Ma) and subglacial during the Oligocene-Miocene Transition (~24 Ma) to a marine depositional setting in the early Miocene and early mid-Miocene before ~14 Ma (VB-6.2, Figures 8a and 10). The transition from a subglacial to marine environment indicates an overall grounding line retreat further to the hinterland between ~24 and ~14 Ma. Data ambiguity means that the exact degree of glacial influence during deposition remains unclear. However, the transition from a coastal/terrestrial (late Oligocene) to a marine setting (early Miocene to late mid-Miocene) suggests increased subsidence of the continental shelf around ~24 Ma, coinciding with generation of tunnel valleys along VB-U6 and U6.1 (Figure 9). This indicates the onset of overdeepening of the continental shelf along the Knox Coast due to glacial load from ice sheets present during the

Oligocene-Miocene Transition. This retreat occurs earlier in Vincennes Bay than in Sabrina Coast, where open marine conditions start in the mid-Miocene.

### 5.4. Reorganization of Ice Flow and Establishment of Stable Oscillating Ice Sheets

The end of the early mid-Miocene (>∼14 Ma) was characterized by three ice advances, depositing thick diamictic wedges across the entire imaged continental shelf, and forming a new paleo-shelf break parallel to the modern one (VB-6.3, 6.4, and 6.5; Figures 4–7). The lack of meltwater features associated with these advances also suggests a potential transition from earlier polythermal to less meltwater-rich erosive ice sheets. This glaciation started the glacially induced progradation of Vincennes Bay continental shelf and most likely initiated after the Middle Miocene Climatic Optimum. These advances were followed by a period of grounding line stability, where the grounded ice sheet extended to the paleo-shelf break, depositing a thick unit of locally aggrading sediments at the beginning of the late mid-Miocene (VB-7.1, Figures 6 and 7). Similar behavior of marine-based grounded ice sheets during the mid-Miocene is documented in the Ross Sea by prograding wedges (Bart & De Santis, 2012; Pérez et al., 2021). The decreasing thickness of these wedges westward on the shelf suggests sediment transport roughly from the south-eastern glacial outlets; likely from Vanderford Glacier. This would suggest a change in the main source region of ice sheets on the continental coast, from the Knox Highlands during the Oligocene-Miocene transition to the ASB in the early to mid-Miocene.

This potential transition of the main ice source during the early EAIS development hints at a more complex glacial history of the region. Vincennes Bay may depend on different glacial systems during changing climatic conditions. A diversion of ice flow on such a large scale may potentially be caused by ice sheet reorganization due to changing climatic condition or bed topography changes, which should be accounted for in paleo-ice sheet modeling. This makes Vincennes Bay an ideal target for future paleo-ice flow investigations. Studies have already suggested the variability in ice flow conditions of the glacial outlets of the ASB, suggesting ice flow piracy between Totten and Vanderford Glacier (McCormack et al., 2023).

The rest of the late mid-Miocene (∼14 to 10.5 Ma) was characterized by glacial progradation parallel to the modern shelf break, caused by frequent grounding line oscillations (Figure 10). A minimum of 14 advances to the paleo-shelf break are indicated by the progradational subsequences. These grounding line oscillations were characterized by glacial retreats, which were followed shortly by a readvance to the paleo-shelf break.

Glacial shelf progradation continued through the late Miocene (minimum seven advances) and into the Pliocene (approximately three advances). The reduction in local aggrading facies suggests shorter periods of ice stability at the shelf break. An increase in slope dip resulted in local slope failure and deposition of MTDs on the continental rise (Figure 6a) from the late mid-Miocene to the Pliocene. This suggests extensive and dynamic ice sheet cover over the entire imaged continental shelf during this time period. Similar outer shelf progradation occurred along the Sabrina Coast during the late Miocene and Pliocene (Donda et al., 2023). The middle to late Miocene in Prydz Bay was dominated by shelf-wide aggradation, with progradation occurring earlier during Oligocene and early Miocene (Cooper et al., 1991; Passchier et al., 2017).

In the Quaternary, the ice sheet at Vincennes Bay retreated, forming a giant GZW on the mid-shelf during grounding line stabilization (Tobisch et al., 2025) (Figure 4b). The crescent shape of this GZW, visible in the bathymetry of Vincennes Bay, indicates that it was formed around the main glacial outlets of the Vanderford and Adams Glacier (Tobisch et al., 2025). This suggests that the main ice flow and sediment transport during this time came from the ASB.

## 6. Conclusion

The first high-resolution and deep-penetrating seismic reflection data from Vincennes Bay reveal the structure, sedimentary, and glacial processes that shaped Vincennes Bay continental shelf from the Late Cretaceous until the Quaternary. Early development of the shelf was characterized by extensive fluvial systems in the Late Cretaceous, Paleocene, and Eocene transitioning to glaciofluvial outwash plains in the late Oligocene. This transition indicates the first occurrence of glaciers in the Vincennes Bay area. Large tunnel valley systems likely originating from the Knox Coastal plain are the first indicators of meltwater-rich grounding line expansions onto the continental shelf during the Oligocene-Miocene Transition (∼24 Ma). Reactivation of these tunnel valleys show at least two ice

advances onto the shelf, with a preferred ice flow direction from the Knox Coastal Plain. These initial advances were followed by an ice sheet retreat inland during the early Miocene and early mid-Miocene (<~24 and >~14 Ma). We interpret that an extensive, oscillating, erosive grounded ice sheet covered almost the entire Vincennes Bay continental shelf from the late mid-Miocene (~14 Ma) to the Pliocene (<5 Ma) with a long-term stable ice extent. During this time, the grounded ice sheet advanced an estimated 30 times to the paleo-shelf break, as indicated by partially eroded, prograding glacial sequences. These advances were likely driven by ice flow from the Vincennes Glacier system, as indicated by the thinning of diamictic wedges toward the western shelf. Our results suggest a reorganization of the glacial flow direction in the transition between earlier meltwater-rich glaciations from the Knox Coastal Plain and later highly erosive ice advances driven by Vanderford Glacier, transporting large amounts of sediment. The transitions observed on the Vincennes Bay shelf make the region an ideal target for further investigation of paleo-ice dynamics and future scientific drilling projects in the as yet under-explored East Antarctic. Our results show that modern ice configurations may not be entirely suitable for paleo-ice sheet reconstructions in complex settings and warmer climates show significantly different ice flow patterns in this region.

## Conflict of Interest

The authors declare no conflicts of interest relevant to this study.

## Availability Statement

Seismic data files of *RV Polarstern* expedition PS141 are available via https://doi.org/10.1594/PANGAEA.988745, https://doi.org/10.1594/PANGAEA.988746, and https://doi.org/10.1594/PANGAEA.988747 (Mühlberger-Krause et al., 2026a, 2026b, 2026c) and Russian expedition RAE-59 are available via https://doi.org/10.1594/PANGAEA.991549, https://doi.org/10.1594/PANGAEA.991550, https://doi.org/10.1594/PANGAEA.991551, https://doi.org/10.1594/PANGAEA.991552, and https://doi.org/10.1594/PANGAEA.991553 (Gandyukhin et al., 2026a, 2026b, 2026c, 2026d, 2026e) at the PANGAEA databank.

**Acknowledgments**
We thank the master and crew of RV Polarstern for their support during expedition PS141. We are grateful to National Collections and Marine Infrastructure of CSIRO in Hobart to make their 600-m seismic streamer available and for their help in installing it for our expedition with special thanks to Andrew Martini, Stephen Thomas, and Shannon Palmer. The authors would like to thank Aspen Technology Inc. for providing seismic software licenses and support. We also thank S&P Global for supplying Kingdom Geoscience Software. We thank Editor U. Röhl and Editor's Assistant M. Ramil for handling this submission, and S. Gulick and one anonymous reviewer for their insightful comments. Funds for this project were contributed by the Deutsche Forschungsgemeinschaft (DFG) in the framework of the DFG Priority Program 1158 Antarktisforschung through Project Grant 522416134, and by Subtopic 2.1 "Warming Climates" of the AWI Research Program "Changing Earth–Sustaining our Future." The study contributes to the Scientific Research Program "Instabilities and Thresholds in Antarctica" (INSTANT) of the Scientific Committee for Antarctic Research (SCAR). The equipment loan and contributions by K. Hochmuth were supported by the Australian Research Council Special Research Initiative, Australian Centre for Excellence in Antarctic Science (Project SR200100008). We acknowledge support by the Open Access publication fund of Alfred-Wegener-Institut Helmholtz-Zentrum für Polar- und Meeresforschung. Open Access funding enabled and organized by Projekt DEAL.

## References

Abreu, V., Sullivan, M., Pirmez, C., & Mohrig, D. (2003). Lateral accretion packages (LAPs): An important reservoir element in deep water sinuous channels. *Marine and Petroleum Geology*, *20*(6–8), 631–648. https://doi.org/10.1016/j.marpetgeo.2003.08.003

Aitken, A. R. A., Betts, P. G., Young, D. A., Blankenship, D. D., Roberts, J. L., & Siegert, M. J. (2016). The Australo-Antarctic Columbia to Gondwana transition. *Gondwana Research*, *29*(1), 136–152. https://doi.org/10.1016/j.gr.2014.10.019

Aitken, A. R. A., Li, L., Kulessa, B., Schroeder, D., Jordan, T. A., Whittaker, J. M., et al. (2023). Antarctic sedimentary basins and their influence on ice-sheet dynamics. *Reviews of Geophysics*, *61*(3), e2021RG000767. https://doi.org/10.1029/2021rg000767

Aitken, A. R. A., & Urosevic, L. (2021). A probabilistic and model-based approach to the assessment of glacial detritus from ice sheet change. *Palaeogeography, Palaeoclimatology, Palaeoecology*, *561*, 110053. https://doi.org/10.1016/j.palaeo.2020.110053

Aitken, A. R. A., Young, D. A., Ferraccioli, F., Betts, P. G., Greenbaum, J. S., Richter, T. G., et al. (2014). The subglacial geology of Wilkes Land, east Antarctica. *Geophysical Research Letters*, *41*(7), 2390–2400. https://doi.org/10.1002/2014gl059405

Bart, P. J. (2003). Were West Antarctic Ice Sheet grounding events in the Ross Sea a consequence of East Antarctic Ice Sheet expansion during the middle Miocene? *Earth and Planetary Science Letters*, *216*(1–2), 93–107. https://doi.org/10.1016/s0012-821x(03)00509-0

Bart, P. J., Anderson, J. B., Trincardi, F., & Shipp, S. S. (2000). Seismic data from the northern basin, Ross Sea, record extreme expansions of the East Antarctic Ice Sheet during the late Neogene. *Marine Geology*, *166*(1–4), 31–50. https://doi.org/10.1016/s0025-3227(00)00006-2

Bart, P. J., & De Santis, L. (2012). Glacial intensification during the Neogene: A review of seismic stratigraphic evidence from the Ross Sea, Antarctica, continental shelf. *Oceanography*, *25*(3), 166–183. https://doi.org/10.5670/oceanog.2012.92

Batchelor, C. L., & Dowdeswell, J. A. (2015). Ice-sheet grounding-zone wedges (GZWs) on high-latitude continental margins. *Marine Geology*, *363*, 65–92. https://doi.org/10.1016/j.margeo.2015.02.001

Batchelor, C. L., Dowdeswell, J. A., & Pietras, J. T. (2014). Evidence for multiple quaternary ice advances and fan development from the Amundsen Gulf cross-shelf trough and slope, Canadian Beaufort Sea margin. *Marine and Petroleum Geology*, *52*, 125–143. https://doi.org/10.1016/j.marpetgeo.2013.11.005

Bellwald, B., Maharjan, D., Planke, S., Winsborrow, M., Rydningen, T. A., Alexandropoulou, N., & Myklebust, R. (2024). Major tunnel valleys and sedimentation changes document extensive early Pleistocene glaciations of the Barents Sea. *Communications Earth & Environment*, *5*(1), 551. https://doi.org/10.1038/s43247-024-01688-x

Bellwald, B., Planke, S., Polteau, S., Lebedeva-Ivanova, N., Faleide, J. I., Morris, S. M., et al. (2021). Characterization of a glacial paleo-outburst flood using high-resolution 3-D seismic data: Bjørnelva River Valley, SW Barents Sea. *Journal of Glaciology*, *67*(263), 404–420. https://doi.org/10.1017/jog.2020.115

Berger, A. L., Gulick, S. P. S., Spotila, J. A., Upton, P., Jaeger, J. M., Chapman, J. B., et al. (2008). Quaternary tectonic response to intensified glacial erosion in an orogenic wedge. *Nature Geoscience*, *1*(11), 793–799. https://doi.org/10.1038/ngeo334

Close, D. I., Stagg, H. M. J., & O'Brien, P. E. (2007). Seismic stratigraphy and sediment distribution on the Wilkes Land and Terre Adelie margins, east Antarctica. *Marine Geology*, *239*(1–2), 33–57. https://doi.org/10.1016/j.margeo.2006.12.010

Cooper, A., Stagg, H., & Geist, E. (1991). Seismic stratigraphy and structure of Prydz Bay, Antarctica: Implications from leg 119 drilling. In *Proceedings of the ocean drilling program, 119 scientific results: Texas A&M university*. Ocean Drilling Program. https://doi.org/10.2973/odp.proc.sr.119.181.1991

De Santis, L. (1999). The eastern Ross Sea continental shelf during the Cenozoic: Implications for the West Antarctic ice sheet development. *Global and Planetary Change*, *23*(1–4), 173–196. https://doi.org/10.1016/s0921-8181(99)00056-9

De Santis, L., Brancolini, G., & Donda, F. (2003). Seismo-stratigraphic analysis of the Wilkes Land continental margin (east Antarctica): Influence of glacially driven processes on the Cenozoic deposition. *Deep Sea Research Part II: Topical Studies in Oceanography*, *50*(8–9), 1563–1594. https://doi.org/10.1016/s0967-0645(03)00079-1

Donda, F., Leitchenkov, G., Brancolini, G., Romeo, R., De Santis, L., Escutia, C., et al. (2020). The influence of Totten Glacier on the Late Cenozoic sedimentary record. *Antarctic Science*, *32*(4), 288–300. https://doi.org/10.1017/s0954102020000188

Donda, F., Romeo, R., Leitchenkov, G., Gei, D., Rosenthal, Y., Leventer, A., et al. (2023). Evidence of the evolution of the East Antarctic Ice Sheet on the continental slope and rise sedimentary record: Insights from the Sabrina Coast, east Antarctica. *GSA Bulletin*. https://doi.org/10.1130/b36674.1

Dong, Y., Zhu, X., Xian, B., Hu, T., Geng, X., Liao, J., & Luo, Q. (2015). Seismic geomorphology study of the Paleogene Hetaoyuan formation, central-south Biyang Sag, Nanxiang Basin, China. *Marine and Petroleum Geology*, *64*, 104–124. https://doi.org/10.1016/j.marpetgeo.2015.02.042

Dorschel, B., Hehemann, L., Viquerat, S., Warnke, F., Dreutter, S., Tenberge, Y. S., et al. (2022). The international bathymetric chart of the southern ocean version 2. *Scientific Data*, *9*(1), 275. https://doi.org/10.1038/s41597-022-01366-7

Easley, G., Labate, D., & Lim, W.-Q. (2008). Sparse directional image representations using the discrete Shearlet transform. *Applied and Computational Harmonic Analysis*, *25*(1), 25–46. https://doi.org/10.1016/j.acha.2007.09.003

Eisen, O., Winter, A., Steinhage, D., Kleiner, T., & Humbert, A. (2020). Basal roughness of the East Antarctic Ice Sheet in relation to flow speed and basal thermal state. *Annals of Glaciology*, *61*(81), 162–175. https://doi.org/10.1017/aog.2020.47

Erohina, T., Cooper, A., Handwerger, D., & Dunbar, R. (2004). Seismic stratigraphic correlations between ODP sites 742 and 1166: Implications for depositional paleoenvironments in Prydz Bay, Antarctica. In *Proceedings of the ocean drilling program* (Vol. 188). Scientific Results. https://doi.org/10.2973/odp.proc.sr.188.011.2004

Escutia, C., Brinkhuis, H., & Klaus, A. (2011). IODP expedition 318: From greenhouse to icehouse at the Wilkes Land Antarctic margin. *Scientific Drilling*, *12*, 15–23. https://doi.org/10.5194/sd-12-15-2011

Escutia, C., Warnke, D., Acton, G. D., Barcena, A., Burckle, L., Canals, M., & Frazee, C. S. (2003). Sediment distribution and sedimentary processes across the Antarctic Wilkes Land margin during the Quaternary. *Deep Sea Research Part II: Topical Studies in Oceanography*, *50*(8–9), 1481–1508. https://doi.org/10.1016/s0967-0645(03)00073-0

Exon, N., Kennett, J., Malone, M., Brinkhuis, H., Chaproniere, G., Ennyu, A., et al. (2011). Drilling reveals climatic consequences of Tasmanian gateway opening. *Eos, Transactions American Geophysical Union*, *83*(23), 253–259. https://doi.org/10.1029/2002eo000176

Fernandez, R., Gulick, S., Domack, E., Montelli, A., Leventer, A., Shevenell, A., & Frederick, B. (2018). Past ice stream and ice sheet changes on the continental shelf off the Sabrina Coast, east Antarctica. *Geomorphology*, *317*, 10–22. https://doi.org/10.1016/j.geomorph.2018.05.020

Galeotti, S., DeConto, R., Naish, T., Stocchi, P., Florindo, F., Pagani, M., et al. (2016). Antarctic ice sheet variability across the Eocene-Oligocene boundary climate transition. *Science*, *352*(6281), 76–80. https://doi.org/10.1126/science.aab0669

Gandyukhin, V., Leitchenkov, G. L., Mühlberger-Krause, T., & Gohl, K. (2026a). 2D multichannel seismic reflection processed data of RV AKADEMIK ALEKSANDR KARPINSKIY during cruise RAE59, Vincennes Bay shelf, profile RAE59-06 [Dataset]. *PANGAEA*. https://doi.org/10.1594/PANGAEA.991549

Gandyukhin, V., Leitchenkov, G. L., Mühlberger-Krause, T., & Gohl, K. (2026b). 2D multichannel seismic reflection processed data of RV AKADEMIK ALEKSANDR KARPINSKIY during cruise RAE59, Vincennes Bay shelf, profile RAE59-06A [Dataset]. *PANGAEA*. https://doi.org/10.1594/PANGAEA.991550

Gandyukhin, V., Leitchenkov, G. L., Mühlberger-Krause, T., & Gohl, K. (2026c). 2D multichannel seismic reflection processed data of RV AKADEMIK ALEKSANDR KARPINSKIY during cruise RAE59, Vincennes Bay shelf, profile RAE59-07 [Dataset]. *PANGAEA*. https://doi.org/10.1594/PANGAEA.991551

Gandyukhin, V., Leitchenkov, G. L., Mühlberger-Krause, T., & Gohl, K. (2026d). 2D multichannel seismic reflection processed data of RV AKADEMIK ALEKSANDR KARPINSKIY during cruise RAE59, Vincennes Bay shelf, profile RAE59-08 [Dataset]. *PANGAEA*. https://doi.org/10.1594/PANGAEA.991552

Gandyukhin, V., Leitchenkov, G. L., Mühlberger-Krause, T., & Gohl, K. (2026e). 2D multichannel seismic reflection processed data of RV AKADEMIK ALEKSANDR KARPINSKIY during cruise RAE59, Vincennes Bay shelf, profile RAE59-09 [Dataset]. *PANGAEA*. https://doi.org/10.1594/PANGAEA.991553

Gibbons, A. D., Whittaker, J. M., & Müller, R. D. (2013). The breakup of east Gondwana: Assimilating constraints from Cretaceous ocean basins around India into a best-fit tectonic model. *Journal of Geophysical Research: Solid Earth*, *118*(3), 808–822. https://doi.org/10.1002/jgrb.50079

Gohl, K., Uenzelmann-Neben, G., Gille-Petzoldt, J., Hillenbrand, C. D., Klages, J. P., Bohaty, S. M., et al. (2021). Evidence for a highly dynamic West Antarctic Ice Sheet during the Pliocene. *Geophysical Research Letters*, *48*(14), e2021GL093103. https://doi.org/10.1029/2021gl093103

Gohl, K., Uenzelmann-Neben, G., Larter, R. D., Hillenbrand, C.-D., Hochmuth, K., Kalberg, T., et al. (2013). Seismic stratigraphic record of the Amundsen Sea embayment shelf from pre-glacial to recent times: Evidence for a dynamic West Antarctic Ice Sheet. *Marine Geology*, *344*, 115–131. https://doi.org/10.1016/j.margeo.2013.06.011

Grollimund, B., & Zoback, M. D. (2000). Post glacial lithospheric flexure and induced stresses and pore pressure changes in the northern North Sea. *Tectonophysics*, *327*(1–2), 61–81. https://doi.org/10.1016/s0040-1951(00)00162-1

Guitard, M. E., Shevenell, A. E., Lavoie, C., & Domack, E. W. (2016). Mega-scale glacial lineations and grounding-zone wedges in Prydz Channel, east Antarctica. *Geological Society, London, Memoirs*, *46*(1), 185–186. https://doi.org/10.1144/m46.110

Gulick, S. P. S., Shevenell, A. E., Montelli, A., Fernandez, R., Smith, C., Warny, S., et al. (2017). Initiation and long-term instability of the East Antarctic Ice Sheet. *Nature*, *552*(7684), 225–229. https://doi.org/10.1038/nature25026

Hochmuth, K., & Gohl, K. (2013). Glaciomarine sedimentation dynamics of the Abbot glacial trough of the Amundsen Sea embayment shelf, west Antarctica. *Geological Society, London, Special Publications*, *381*(1), 233–244. https://doi.org/10.1144/sp381.21

Hochmuth, K., Gohl, K., Leitchenkov, G., Sauermilch, I., Whittaker, J. M., Uenzelmann-Neben, G., et al. (2020). The evolving paleobathymetry of the circum-Antarctic Southern Ocean since 34 ma: A key to understanding past cryosphere-ocean developments. *Geochemistry, Geophysics, Geosystems*, *21*(8), e2020GC009122. https://doi.org/10.1029/2020gc009122

Jamieson, S. S. R., Ross, N., Paxman, G. J. G., Clubb, F. J., Young, D. A., Yan, S., et al. (2023). An ancient river landscape preserved beneath the East Antarctic Ice Sheet. *Nature Communications*, *14*(1), 6507. https://doi.org/10.1038/s41467-023-42152-2

Jobe, Z. R., Howes, N. C., & Auchter, N. C. (2016). Comparing submarine and fluvial channel kinematics: Implications for stratigraphic architecture. *Geology*, *44*(11), 931–934. https://doi.org/10.1130/g38158.1

Jørgensen, F., & Sandersen, P. B. E. (2006). Buried and open tunnel valleys in Denmark—erosion beneath multiple ice sheets. *Quaternary Science Reviews*, *25*(11–12), 1339–1363. https://doi.org/10.1016/j.quascirev.2005.11.006

Kehew, A. E., Piotrowski, J. A., & Jørgensen, F. (2012). Tunnel valleys: Concepts and controversies — A review. *Earth-Science Reviews*, *113*(1–2), 33–58. https://doi.org/10.1016/j.earscirev.2012.02.002

Kirkham, J. D., Hogan, K. A., Larter, R. D., Arnold, N. S., Ely, J. C., Clark, C. D., et al. (2024). Tunnel valley formation beneath deglaciating mid-latitude ice sheets: Observations and modelling. *Quaternary Science Reviews*, *323*, 107680. https://doi.org/10.1016/j.quascirev.2022.107680

Klages, J. P., Hillenbrand, C. D., Bohaty, S. M., Salzmann, U., Bickert, T., Lohmann, G., et al. (2024). Ice sheet–free west Antarctica during peak early Oligocene glaciation. *Science*, *385*(6706), 322–327. https://doi.org/10.1126/science.adj3931

Klages, J. P., Kuhn, G., Hillenbrand, C. D., Smith, J. A., Graham, A. G. C., Nitsche, F. O., et al. (2017). Limited grounding-line advance onto the west Antarctic continental shelf in the easternmost Amundsen Sea embayment during the last glacial period. *PLoS One*, *12*(7), e0181593. https://doi.org/10.1371/journal.pone.0181593

Krastel, S. (2025). The expedition PS141 of the research vessel POLARSTERN to the Davis Sea and Mawson Sea in 2024, A.-W.-I. H.-Z. f. P.-u. Meeresforschung. https://doi.org/10.57738/BzPM_0793_2025

Kristensen, T. B., Piotrowski, J. A., Huuse, M., Clausen, O. R., & Hamberg, L. (2008). Time-transgressive tunnel valley formation indicated by infill sediment structure, North Sea – The role of glaciohydraulic supercooling. *Earth Surface Processes and Landforms*, *33*(4), 546–559. https://doi.org/10.1002/esp.1668

Landschulze, K., & Landschulze, M. (2021). Fracture formation due to differential compaction under glacial load: A poro-elastoplastic simulation of the Hugin fracture. *Marine Geophysical Researches*, *42*(1), 1. https://doi.org/10.1007/s11001-020-09422-w

Leitchenkov, G. L., Gandyukhin, V. V., Guseva, Y. B., & Kazankov, A. Y. (2007). Crustal structure and evolution of the Mawson Sea, western Wilkes Land margin, east Antarctica. In *Paper presented at the 10th int. Symp. on Antarctic Earth science*. https://doi.org/10.3133/of2007-1047.srp028

Leitchenkov, G. L., Guseva, K., Gandyukhin, V., & Ivanov, S. (2015). *Crustal structure, tectonic evolution and seismic stratigraphy of the southern Indian Ocean*. VNIIOkeangeologia.

Li, X., Rignot, E., Mouginot, J., & Scheuchl, B. (2016). Ice flow dynamics and mass loss of Totten Glacier, east Antarctica, from 1989 to 2015. *Geophysical Research Letters*, *43*(12), 6366–6373. https://doi.org/10.1002/2016gl069173

Lim, W. Q. (2010). The discrete shearlet transform: A new directional transform and compactly supported shearlet frames. *IEEE Transactions on Image Processing*, *19*(5), 1166–1180. https://doi.org/10.1109/TIP.2010.2041410

Lohrberg, A., Schwarzer, K., Unverricht, D., Omlin, A., & Krastel, S. (2020). Architecture of tunnel valleys in the southeastern North Sea: New insights from high-resolution seismic imaging. *Journal of Quaternary Science*, *35*(7), 892–906. https://doi.org/10.1002/jqs.3244

Lonergan, L., Maidment, S. C. R., & Collier, J. S. (2006). Pleistocene subglacial tunnel valleys in the central North Sea basin: 3-D morphology and evolution. *Journal of Quaternary Science*, *21*(8), 891–903. https://doi.org/10.1002/jqs.1015

Maritati, A., Aitken, A. R. A., Young, D. A., Roberts, J. L., Blankenship, D. D., & Siegert, M. J. (2016). The tectonic development and erosion of the Knox subglacial sedimentary basin, east Antarctica. *Geophysical Research Letters*, *43*(20), 10728–10737. https://doi.org/10.1002/2016gl071063

Maritati, A., Danišík, M., Halpin, J. A., Whittaker, J. M., & Aitken, A. R. A. (2020). Pangea rifting shaped the east Antarctic landscape. *Tectonics*, *39*(8), e2020TC006180. https://doi.org/10.1029/2020tc006180

McCormack, F. S., Roberts, J. L., Kulessa, B., Aitken, A., Dow, C. F., Bird, L., et al. (2023). Assessing the potential for ice flow piracy between the Totten and Vanderford Glaciers, east Antarctica. *The Cryosphere*, *17*(11), 4549–4569. https://doi.org/10.5194/tc-17-4549-2023

McKay, R. M., Cockrell, J., Shevenell, A. E., Laberg, J. S., Burns, J., Patterson, M., et al. (2024). Miocene ice sheet dynamics and sediment deposition in the central Ross Sea, Antarctica. *Geological Society of America Bulletin*, *137*(3–4), 1267–1291. https://doi.org/10.1130/b37613.1

McKay, R. M., Escutia, C., De Santis, L., Donda, F., Duncan, B., Gohl, K., et al. (2022). Cenozoic history of Antarctic glaciation and climate from onshore and offshore studies. In *Antarctic climate evolution* (pp. 41–164). https://doi.org/10.1016/b978-0-12-819109-5.00008-6

Montelli, A., Gulick, S. P. S., Fernandez, R., Frederick, B. C., Shevenell, A. E., Leventer, A., & Blankenship, D. D. (2020). Seismic stratigraphy of the Sabrina Coast shelf, east Antarctica: Early history of dynamic meltwater-rich glaciations. *Geological Society of America Bulletin*, *132*(3–4), 545–561. https://doi.org/10.1130/B35100.1

Morlighem, M., Rignot, E., Binder, T., Blankenship, D., Drews, R., Eagles, G., et al. (2020). Deep glacial troughs and stabilizing ridges unveiled beneath the margins of the Antarctic ice sheet. *Nature Geoscience*, *13*(2), 132–137. https://doi.org/10.1038/s41561-019-0510-8

Mühlberger-Krause, T., Gohl, K., Hochmuth, K., Barrett, R., Tobisch, C. A., & Krastel, S. (2026a). 2D multichannel seismic reflection processed data of RV POLARSTERN during cruise PS141, Vincennes Bay shelf, profile AWI-20240009 [Dataset]. *PANGAEA*. https://doi.org/10.1594/PANGAEA.988745

Mühlberger-Krause, T., Gohl, K., Hochmuth, K., Barrett, R., Tobisch, C. A., & Krastel, S. (2026b). 2D multichannel seismic reflection processed data of RV POLARSTERN during cruise PS141, Vincennes Bay shelf, profile AWI-20240010 [Dataset]. *PANGAEA*. https://doi.org/10.1594/PANGAEA.988746

Mühlberger-Krause, T., Gohl, K., Hochmuth, K., Barrett, R., Tobisch, C. A., & Krastel, S. (2026c). 2D multichannel seismic reflection processed data of RV POLARSTERN during cruise PS141, Vincennes Bay shelf, profile AWI-20240011 [Dataset]. *PANGAEA*. https://doi.org/10.1594/PANGAEA.988747

O'Brien, P. E., Cooper, A. K., Florindo, F., Handwerger, D., Lavelle, M., Passchier, S., et al. (2004). Prydz channel fan and the history of extreme ice advances in Prydz Bay. In *Proceedings of the ocean drilling program* (Vol. 188). Scientific Results. https://doi.org/10.2973/odp.proc.sr.188.016.2004

Passchier, S., Ciarletta, D. J., Miriagos, T. E., Bijl, P. K., & Bohaty, S. M. (2017). An Antarctic stratigraphic record of stepwise ice growth through the Eocene-Oligocene transition. *Geological Society of America Bulletin*, *129*(3–4), 318–330. https://doi.org/10.1130/b31482.1

Paxman, G. J. G. (2021). Antarctic palaeotopography. *Geological Society, London, Memoirs*, *56*(1), 231–251. https://doi.org/10.1144/m56-2020-7

Paxman, G. J. G., Jamieson, S. S. R., Hochmuth, K., Gohl, K., Bentley, M. J., Leitchenkov, G., & Ferraccioli, F. (2019). Reconstructions of Antarctic topography since the Eocene–Oligocene boundary. *Palaeogeography, Palaeoclimatology, Palaeoecology*, *535*, 109346. https://doi.org/10.1016/j.palaeo.2019.109346

Paxman, G. J. G., Jamieson, S. S. R., Ross, N., Bentley, M. J., Carter, C. M., Jordan, T. A., et al. (2025). Extensive fluvial surfaces at the east Antarctic margin have modulated ice-sheet evolution. *Nature Geoscience*, *18*(8), 724–731. https://doi.org/10.1038/s41561-025-01734-z

Pelle, T., Morlighem, M., & McCormack, F. S. (2020). Aurora basin, the weak underbelly of east Antarctica. *Geophysical Research Letters*, *47*(9), e2019GL086821. https://doi.org/10.1029/2019gl086821

Pelle, T., Morlighem, M., Nakayama, Y., & Seroussi, H. (2021). Widespread grounding line retreat of Totten glacier, east Antarctica, over the 21st century. *Geophysical Research Letters*, *48*(17), e2021GL093213. https://doi.org/10.1029/2021gl093213

Pérez, L. F., Santis, L. D., McKay, R. M., Larter, R. D., Ash, J., Bart, P. J., et al. (2021). Early and middle Miocene ice sheet dynamics in the Ross Sea: Results from integrated core-log-seismic interpretation. *GSA Bulletin*, *134*(1–2), 348–370. https://doi.org/10.1130/b35814.1

Picton, H. J., Stokes, C. R., Jamieson, S. S. R., Floricioiu, D., & Krieger, L. (2023). Extensive and anomalous grounding line retreat at Vanderford Glacier, Vincennes Bay, Wilkes Land, east Antarctica. *The Cryosphere*, *17*(8), 3593–3616. https://doi.org/10.5194/tc-17-3593-2023

Powell, R. D., & Cooper, J. M. (2003). A glacial sequence stratigraphic model for temperate, glaciated continental shelves. *Geological Society, London, Special Publications*, *203*(1), 215–244. https://doi.org/10.1144/gsl.Sp.2002.203.01.12

Sauermilch, I., Whittaker, J. M., Bijl, P. K., Totterdell, J. M., & Jokat, W. (2019). Tectonic, oceanographic, and climatic controls on the cretaceous-Cenozoic sedimentary record of the Australian-Antarctic basin. *Journal of Geophysical Research: Solid Earth*, *124*(8), 7699–7724. https://doi.org/10.1029/2018jb016683

Scher, H. D., Whittaker, J. M., Williams, S. E., Latimer, J. C., Kordesch, W. E., & Delaney, M. L. (2015). Onset of Antarctic circumpolar current 30 million years ago as Tasmanian gateway aligned with westerlies. *Nature*, *523*(7562), 580–583. https://doi.org/10.1038/nature14598

Ship, S., Anderson, J., & Domack, E. (1999). Late Pleistocene–Holocene retreat of the west Antarctic ice-sheet system in the Ross Sea: Part 1—Geophysical results. *Geological Society of America Bulletin*, *111*(10), 1486. https://doi.org/10.1130/0016-7606(1999)111<1486:Lphrot>2.3.Co;2

Smith, B., Fricker, H. A., Gardner, A. S., Medley, B., Nilsson, J., Paolo, F. S., et al. (2020). Pervasive ice sheet mass loss reflects competing ocean and atmosphere processes. *Science*, *368*(6496), 1239–1242. https://doi.org/10.1126/science.aaz5845

Stewart, M. A., Lonergan, L., & Hampson, G. (2013). 3D seismic analysis of buried tunnel valleys in the central North Sea: Morphology, cross-cutting generations and glacial history. *Quaternary Science Reviews*, *72*, 1–17. https://doi.org/10.1016/j.quascirev.2013.03.016

Stokes, C. R., Abram, N. J., Bentley, M. J., Edwards, T. L., England, M. H., Foppert, A., et al. (2022). Response of the East Antarctic Ice Sheet to past and future climate change. *Nature*, *608*(7922), 275–286. https://doi.org/10.1038/s41586-022-04946-0

Tobisch, C. A., Barrett, R., Klages, J., Hochmuth, K., Mühlberger-Krause, T., Gohl, K., et al. (2025). A giant grounding zone wedge in Vincennes Bay, east Antarctica: Geomorphological characteristics and internal structure. In *Paper presented at the EGU general assembly 2025*.

Verschuur, D. J., Berkhout, A. J., & Wapenaar, C. P. A. (1992). Adaptive surface-related multiple elimination. *Geophysics*, *57*(9), 1166–1177. https://doi.org/10.1190/1.1443330

Wang, G., Huang, X., Liu, S., Wu, S., & Ma, Z. (2024). The role of ice-sheet dynamics in the Miocene-Pliocene depositional systems of the Ross Sea, Antarctica. *Palaeogeography, Palaeoclimatology, Palaeoecology*, *648*, 112253. https://doi.org/10.1016/j.palaeo.2024.112253

Wang, Y., Lin, C., Zhang, Z., Zhang, B., & Liu, H. (2021). Sedimentary evolution and controlling factors of early-mid Miocene Deltaic systems in the Northern Pearl River Mouth Basin, South China Sea. *Scientific Reports*, *11*(1), 6134. https://doi.org/10.1038/s41598-021-85369-1

Weigelt, E., Uenzelmann-Neben, G., Gohl, K., & Larter, R. D. (2012). Did massive glacial dewatering modify sedimentary structures on the Amundsen Sea Embayment shelf, west Antarctica? *Global and Planetary Change*, *92–93*, 8–16. https://doi.org/10.1016/j.gloplacha.2012.04.006

Whittaker, J. M., Muller, R. D., Leitchenkov, G., Stagg, H., Sdrolias, M., Gaina, C., & Goncharov, A. (2007). Major Australian-Antarctic plate reorganization at Hawaiian-emperor bend time. *Science*, *318*(5847), 83–86. https://doi.org/10.1126/science.1143769

Williams, S. E., Whittaker, J. M., Halpin, J. A., & Müller, R. D. (2019). Australian-Antarctic breakup and seafloor spreading: Balancing geological and geophysical constraints. *Earth-Science Reviews*, *188*, 41–58. https://doi.org/10.1016/j.earscirev.2018.10.011

Young, D. A., Wright, A. P., Roberts, J. L., Warner, R. C., Young, N. W., Greenbaum, J. S., et al. (2011). A dynamic early East Antarctic Ice Sheet suggested by ice-covered fjord landscapes. *Nature*, *474*(7349), 72–75. https://doi.org/10.1038/nature10114

Zundel, M., Spiegel, C., Mark, C., Millar, I., Chew, D., Klages, J., et al. (2024). A large-scale transcontinental river system crossed west Antarctica during the Eocene. *Science Advances*, *10*(23), eadn6056. https://doi.org/10.1126/sciadv.adn6056